

ADAPTIVE ROLL CONTROL OF GUIDED MUNITIONS

A THESIS SUBMITTED TO
THE GRADUATE SCHOOL OF NATURAL AND APPLIED SCIENCES
OF
MIDDLE EAST TECHNICAL UNIVERSITY

BY

NAZ TUĞÇE ÖVEÇ

IN PARTIAL FULFILLMENT OF THE REQUIREMENTS
FOR
THE DEGREE OF MASTER OF SCIENCE
IN
AEROSPACE ENGINEERING

JANUARY 2016

Approval of the thesis

ADAPTIVE ROLL CONTROL OF GUIDED MUNITIONS

submitted by **NAZ TUĞÇE ÖVEÇ** in partial fulfillment of the requirements for the degree of **Master of Science in Aerospace Engineering Department, Middle East Technical University** by,

Prof. Dr. Gülbin Dural Ünver
Dean, Graduate School of **Natural and Applied Sciences**

Prof. Dr. Ozan Tekinalp
Head of Department, **Aerospace Engineering**

Asst. Prof. Dr. Ali Türker Kutay
Supervisor, **Aerospace Engineering Dept.,METU**

Examining Committee Members:

Prof. Dr. Ozan Tekinalp
Aerospace Engineering Dept.,METU

Asst. Prof. Dr. Ali Türker Kutay
Aerospace Engineering Dept.,METU

Prof. Dr. M. Kemal Leblebicioğlu
Electrical and Electronics Engineering Dept.,METU

Assoc. Prof. Dr. İlkay Yavrucuk
Aerospace Engineering Dept.,METU

Assoc. Prof. Dr. Coşku Kasnakoğlu
Electrical and Electronics Engineering Dept.,TOBB UET

Date: _____

I hereby declare that all information in this document has been obtained and presented in accordance with academic rules and ethical conduct. I also declare that, as required by these rules and conduct, I have fully cited and referenced all material and results that are not original to this work.

Name, Last name : NAZ TUĞÇE ÖVEÇ

Signature :

ABSTRACT

ADAPTIVE ROLL CONTROL OF GUIDED MUNITIONS

Öveç, Naz Tuğçe

M.S., Department of Aerospace Engineering

Supervisor: Asst. Prof. Dr. Ali Türker Kutay

January 2016, 90 Pages

This thesis presents an adaptive roll control scheme for guided munitions. Guided munitions are air-to-air or air-to-surface weapons which have enhanced target hit capabilities with laser seekers or similar guidance utilities. The dynamic interferences in nonlinear regions of the flight envelope, leads the studies on control of guided munitions to search for adaptive solutions. The missile used in this study has no propulsive forces and do the adequate maneuvers commanded by the guidance algorithm with its initial kinetic and potential energy.

In this study first, the baseline roll autopilot is developed which is in cascaded two loop architecture augmented with a feedforward controller and a model reference controller structure. Since the coupling effects could not be eliminated with the baseline architecture, the control algorithm is improved with a model reference adaptive controller with Chebyshev polynomials based uncertainty parameterization. Then the study is extended by utilizing concurrent learning algorithm as the adaptation law to learn and reveal the unknown pitch-roll couplings.

Keywords: Concurrent Learning Adaptive Control, Uncertainty Parameterization with Chebyshev Polynomials, Control of Guided Munitions

ÖZ

GÜDÜM KİTİ TİPİ MÜHİMMATLARIN ADAPTİF YUVARLANMA KANALI KONTROLÜ

Öveç, Naz Tuğçe

Yüksek Lisans, Havacılık ve Uzay Mühendisliği Bölümü

Tez Yöneticisi: Yrd. Doç. Dr. Ali Türker Kutay

Ocak 2016, 90 Sayfa

Bu tez güdüm kiti mühimmatların adaptif yuvarlanma kanalı kontrolü üzerine yapılan çalışmayı içermektedir. Güdüm kiti tipi mühimmatlar havadan havaya veya havadan karaya, hedef vurma kabiliyetleri lazer arayıcı başlık veya benzeri güdüm kitleriyle arttırılmış bombalardır. Bu mühimmatların uçuş zarfının doğrusal olmayan bölgelerindeki eksenler arası etkileşimler, kontrol probleminin çözüm uzayını adaptif kontrolcülere doğru genişletmiştir. Bu çalışmada kullanılan füze, motoru ve itki kuvveti bulunmayan ve güdüm algoritmasının ürettiği komutları ayrılma anındaki kinetik ve potansiyel enerjisi yardımıyla yardımcıyla gerçekleyen bir Mk-82 bomba türevidir.

Bu çalışmada öncelikle, ara değerlendirme prensibiyle çalışan iki döngülü yuvarlanma açısı kontrolcüsü ve onun ileri besleme kontrolcüsüyle güncellenmiş versiyonu ayrıca model takip eden kontrolcü yapıları ele alınmıştır. Dönü kanalına sirayet eden dinamik etkileşimler bu temel tasarımlarla bastırılamamış ve belirsizlik parametrizasyonu Chebyshev polinom açılımları ile yapılan model takip eden adaptif kontrolcülerle bu bozucu etki ortadan kaldırılmıştır. Çalışmanın devamı olarak da geçmiş ve güncel bilgileri kullanarak belirsizliği eşyönlü öğrenen bir algoritma ile model takip eden adaptif kontrolcü güncellenmiş ve bilinmeyen yuvarlanma-yunuslama kanalı belirsizliklerine ait bir model elde edilebilmiştir.

Anahtar Kelimeler: Eşyönlü Öğrenen Adaptif Kontrolcü, Güdümlü Bomba, Chebyshev Polinomlarıyla Belirsizlik Parametrizasyonu

To my mother and father with love and gratitude

ACKNOWLEDGEMENTS

I would like to begin with expressing my sincere gratitude to my supervisor Asst. Dr. Ali Türker Kutay for being supportive, well-disposed and having me so welcomed all the time. I owe lots of thanks to him for all valuable discussions, guiding me through and endeavoring hard for me to prosper this work.

I would like to thank Assoc. Dr. İlkey Yavrucuk for encouraging and supporting me in the beginning of my thesis studies. I would also like to present my acknowledgements to my project leader Gökhan Tüşün for his invaluable trust in me throughout the times we have worked together and to my colleagues Berna Ünal and Evrim Özten for their valuable helps and support.

I am forever indebted to my very close friends Suzan Kale Güvenç and Sogand Yousefbeigi for enlightening me whenever I got lost in questions and encouraging me right from the beginning.

I am forever grateful to my parents Güler Öveç and Fahrettin Öveç close to me all the time more than anyone with their endless support, love and faith in me. I would like to extend my thanks to each of my aunts, uncles, cousins, and grandparents. Without them it would all be for naught.

Last, I want to express my deepest gratitude to Görkem Eşsiz for his never ending support, patience and invaluable endeavor. I will always be grateful to him for standing by me through all the tough times of this phase.

TABLE OF CONTENTS

ABSTRACT	v
ÖZ	vi
ACKNOWLEDGEMENTS	viii
TABLE OF CONTENTS	ix
LIST OF FIGURES	xi
LIST OF ABBREVIATIONS.....	xiv
CHAPTERS	
1. INTRODUCTION	1
1.1 Motivation.....	1
1.2 Literature Review.....	3
1.3 Contributions of This Thesis.....	6
1.4 Organization of the Thesis	7
2. MISSILE DYNAMICS AND CHARACTERISTICS.....	9
2.1 Coordinate Systems.....	9
2.2 Rigid Body Equations of Motion	11
2.3 Aerodynamic Forces and Moments	13
2.4 Gravitational Forces	15
2.5 Missile Characteristics	15
3. BASELINE ROLL AUTOPILOT AUGMENTATIONS	17
3.1 Cascaded Roll Autopilot Design.....	18
3.2 Roll Autopilot Augmentation with Feedforward Controller.....	19
3.3 Fixed Gain Model Reference Controller Design for Roll Channel	24
4. ADAPTIVE ROLL AUTOPILOT DESIGN	29
4.1 Why Adaptive Control?	30
4.2 Uncertainty Parameterization Independent of the System States	30
4.3 Model Reference Adaptive Controller Design for Roll Channel.....	32

4.3.1	Tracking Error Dynamics	34
4.3.2	Adaptive Controller Design	35
4.4	Concurrent Learning Model Reference Adaptive Control.....	43
4.4.1	Concurrent Learning Weight Update Law.....	45
4.4.2	Data Selection Algorithm for the History Stack.....	46
4.4.3	Effect of the Span of Basis and History Stack Size on Learning..	52
5.	SIMULATION RESULTS.....	55
5.1	Roll Control of the Guided Munition with Baseline Roll Autopilot during Compelling Longitudinal Maneuvers	55
5.1.1	Roll Control with Cascaded Autopilot.....	55
5.1.2	Roll Control with MRC	61
5.2	Adaptive Roll Control of the Guided Munition during Compelling Longitudinal Maneuvers	62
5.2.1	Roll Control with Classical MRAC	62
5.2.2	Roll Control with Concurrent Learning Aided MRAC	64
5.2.3	Comparison of the State Dependent Uncertainty Parametrization with the Angle of Attack Based Uncertainty Parameterization	69
5.2.4	Verification of the Uncertainty Model.....	72
6.	CONCLUSION AND FUTURE WORK.....	75
	REFERENCES.....	79
APPENDICES		
A.	BASELINE AUTOPILOT DESIGN.....	85
A.1	Linear Model Construction	85
A.2	Autopilot Design	87
A.2.1	Acceleration Autopilot Design for Longitudinal and Lateral Planes	88

LIST OF FIGURES

FIGURES

Figure 2.1-1 Orientation of the missile axes with respect to the Earth-fixed axes	10
Figure 2.5-1 Layout of Mk-82 General Purpose Low Drag (GPLD) 500 lb bomb (all dimensions in mm).....	15
Figure 3.1-1 The baseline roll autopilot structure	18
Figure 3.2-1 Variation of Roll Moment Coefficient with α at $0^\circ \beta$	20
Figure 3.2-2 Variation of Roll Moment Coefficient with α at $0 \delta_a$	20
Figure 3.2-3 The linear test model for roll autopilot.....	22
Figure 3.2-4 Linear Simulation Roll Rate Responses of the Cascaded Roll Autopilot with and without Feedforward Controller.....	23
Figure 3.2-5 Linear Simulation Roll Angle Responses of the Cascaded Roll Autopilot with and without Feedforward Controller	23
Figure 3.3-1 Model Reference Controller Structure	26
Figure 3.3-2 Linear Simulation Roll Angle Responses of Model Reference Controller	26
Figure 3.3-3 Linear Simulation Roll Rate Responses of Model Reference Controller	27
Figure 4.3-1 Model Reference Adaptive Controller Structure.....	40
Figure 4.3-2 Linear Simulation Roll Angle, Roll Rate and the Angle of Attack Responses of the MRAC.....	41
Figure 4.3-3 Structured Uncertainty and the Adaptive Control Input Histories	41
Figure 4.3-4 Adaptive Weight Histories of the MRAC	42
Figure 4.4-1 Singular Value Maximizing Algorithm Flow Chart	48
Figure 4.4-2 Linear Simulation Roll Angle, Roll Rate and Angle of Attack Responses of Concurrent Learning MRAC	48

Figure 4.4-3 Structured Uncertainty and Adaptive Control Input Histories of Concurrent Learning MRAC.....	49
Figure 4.4-4 Adaptive Weight Histories of Concurrent Learning MRAC.....	50
Figure 4.4-5 Rank of the History Stack.....	50
Figure 4.4-6 Minimum Singular Value of the History Stack.....	51
Figure 4.4-7 Effects of Basis Span and History Stack Size on Learning.....	53
Figure 5.1-1 Flight Path of the Munition	56
Figure 5.1-2 Elevation Angle Profile of the Munition	56
Figure 5.1-3 Mach Profile of the Munition	57
Figure 5.1-4 Cascaded A/P Longitudinal Acceleration Responses.....	57
Figure 5.1-5 Cascaded A/P Lateral Acceleration Responses for Case-1 and Case-2	58
Figure 5.1-6 Cascaded A/P Angle of Attack Histories for Case-1 and Case-2.....	58
Figure 5.1-7 Cascaded A/P Side Slip Angle Histories for Case-1 and Case-2	59
Figure 5.1-8 Cascaded A/P Roll Angle Responses for Case-1 and Case-2	59
Figure 5.1-9 Cascaded A/P Roll Rate Responses for Case-1 and Case-2.....	60
Figure 5.1-10 MRC Roll Angle Responses.....	61
Figure 5.1-11 MRC Roll Rate Responses	61
Figure 5.2-1 MRAC Roll Angle Responses	63
Figure 5.2-2 MRAC Roll Rate Responses	63
Figure 5.2-3 MRAC Adaptive Weight Histories	64
Figure 5.2-4 Concurrent Learning MRAC Roll Angle Responses	64
Figure 5.2-5 Concurrent Learning MRAC Roll Rate Responses.....	65
Figure 5.2-6 Aileron Command and Response	65
Figure 5.2-7 Concurrent Learning MRAC Minimum Singular Value of the History Stack.....	66
Figure 5.2-8 Concurrent Learning MRAC Rank of the History Stack	67
Figure 5.2-9 Concurrent Learning MRAC Adaptive Controller Weights	68
Figure 5.2-10 The Uncertainty Function Learned from Nonlinear and Linear Simulations.....	69

Figure 5.2-11 Roll Angle Responses with the State Dependent Uncertainty Parameterization.....	70
Figure 5.2-12 Roll Rate Responses with the State Dependent Uncertainty Parameterization.....	71
Figure 5.2-13 Weight Histories with State Dependent Uncertainty Parameterization	71
Figure 5.2-14 Verification of the Uncertainty Model	72
Figure 5.2-15 Rolling Moment Coefficient Histories with Linear, Nonlinear and Modified Linear Databases	73
Figure 5.2-16 Roll Angle Responses with Modified Linear and Nonlinear Databases	74
Figure A.2-1 Control scheme for longitudinal acceleration autopilot	88
Figure A.2-2 The pole-zero map for acceleration autopilot.....	90

LIST OF ABBREVIATIONS

MRC	Model Reference Control
CAS	Control Actuation System
MRAC	Model Reference Adaptive Control
PE	Persistent Excitation
WCC	Weight Convergence Condition

CHAPTER 1

INTRODUCTION

1.1 Motivation

There has been an increasing demand for affordable aerial vehicles with superior performances which leads the missile studies to the design of more agile missiles with relatively low costs. As a part of this rising trend, traditional iron bombs have been modified for more precision on target hit and longer guided flights. These types of weapons are called as guided munitions: air to surface or air-to-air weapons which have been upgraded with a guidance kit for improved target hit capability. These munitions are designed as a family of weapons with minor differences by combining various components around the same body. The guided bombs meet the desired performance requirements with their disengagement velocities mostly in a nonlinear flight envelope due to drastic maneuvers with high angles of attack. As a result, these highly nonlinear flight regimes bring about the dynamic interferences and couplings among roll, pitch and yaw axes. On this basis, the need arises for a controller which is able to overcome dynamic couplings and handle several different configurations without compromising performance.

A flight control problem is usually approached with linear control theory, firstly. The linear controllers that are designed locally are applied to the nonlinear problems with gain scheduling technique which requires large tables of data. The performance of a linear controller is granted only around a restricted local area which is the major problem of linear control theory. To overcome this issue numbers of design points are increased and it brings about a substantial effort to find the controller gains for all design points. Besides, these gains usually need an update to preserve the controller

performance if the plant undergoes some improvements during its utilization time. These issues of the linear control theory lead the control studies through the robust, nonlinear and especially adaptive control solutions, recently.

The adaptive control theory emerged in 1950s with the need for active control of agile aircrafts. The milestone of the adaptive control studies was the stability guarantee of the controller which is proven by Narendra in 80s [1] using Lyapunov stability theory. Adaptive controllers have distinguished in time with the flexibility they offer in modelling and uncertain environments. Especially in flight control applications, a significant effort must be spent to obtain an accurate model of the aerial platform which begins with modelling the system using basic principles and goes up to the system identification and model verification. Even if an adequately accurate model is obtained, it is usually in a nonlinear and coupled form and it becomes impossible to work with a single linear controller that is efficient on the whole operating domain. Nonlinear controllers are generated based on the nonlinear model of the system and consequently they are also dependent on the model's accuracy. Moreover, it is hard to assess the performance of the controller since the well-known indicators such as transient response characteristics could not be easily extracted from the nonlinear content. The robust controllers like the adaptive controllers do not need restrictively accurate plant models; nevertheless they are conservative and this situation brings about performance issues.

The inspiration for this study emerged on this basis to find genuine adaptive solutions for roll control of air -to-surface guided munitions. The research begins with linear control solutions which constitutes a base for more complex approaches and concludes with the proposition of an adaptive autopilot structure.

1.2 Literature Review

Flight control of guided munitions is a challenging problem which leads the designers to search for smart control solutions due to the operating envelope of the weapon with wide dynamic pressure, Mach number and altitude ranges. Additionally the dynamics of these munitions tends to be highly nonlinear due to separation-dominated flow. These problems make the adaptive solutions suitable candidates for handling the flight control of the munitions. Instead of developing a fixed controller over a space of model uncertainty, adaptive control adjusts the controller online based on detections of plant deviations from a reference model. Adaptive control augments and further extends the performance and robustness of the flight control system.

The original concept of adaptive control was proposed by Whitaker et al. [2]. The main idea was specifying the desired response of a system by means of tracking a reference model which was later called the explicit model following control and the architecture became known as model reference adaptive controller (MRAC). Modern adaptive controllers are mainly classified as direct and indirect adaptive controllers. Direct adaptive controllers response fast and track the reference model efficiently whereas they suffer from short time learning since they are not focused on estimating the uncertainty. Their tracking performance might not enhance even though the same command is tracked repeatedly. On the contrary, indirect controllers are designed to identify uncertainty and their tracking performance improves eventually. However, this dependency on the plant dynamics estimation could degrade their transient performance and makes it hard to guarantee performance and stability.

The widely studied class of direct adaptive control methods is known as model reference adaptive control (MRAC) [3]–[6]. In MRAC, the plant is forced to track a reference model which characterizes the desired response. Many physical examples could be found in the literature that involves control using MRAC approaches such as, flight vehicle control [7], [8], or robotic arms [9]. Most MRAC methods achieve

the reference model tracking by using a parameterized model of the uncertainty which is also named as the adaptive weights or the adaptive element. Adaptive elements in MRAC are classified as the ones that are designed to cancel structured uncertainties and the others that are designed for unstructured uncertainties. If the uncertainty is structured, a known basis used to parameterize the uncertainty [10]. If the structure of the uncertainty is unknown but it is defined over a compact domain and continuous, Neural Networks (NN) are used commonly to parameterize the uncertainty [11]–[15]. The universal approximation property of NNs guarantees the optimal approximation of the uncertainty with a bounded error. MRAC scheme ensures asymptotic command tracking despite the system uncertainties but achieving smooth transients or having adaptive parameters converge to their ideal values are not formulated as the design goals. Nevertheless, there are cases when parameter convergence takes place alongside the desired tracking. A sufficient condition for parameter convergence is given by the persistency of excitation (PE) which imposes certain restrictions on the reference command signal. However, the condition on PE reference input is often not feasible or hard to monitor online. In order to guarantee robustness and uncertainty elimination without PE reference inputs, various methods have been offered such as the σ -modification [16] and the e -modification [10]. These methods ensure that the adaptive weights do not diverge even when the PE condition is violated. But the increased damping on the weights due to these terms could prevent the learning and convergence of the weights [17]. The weight convergence benefits in many ways to the system. It indicates exponential error convergence, uniform approximation of the plant uncertainty and the guaranteed exponentially bounded transient performance. Uniformly cancelled uncertainty let the plant track the reference model exponentially which means that reference model and the plant responses become indistinguishable at some point. Hence, it would be possible to assess the performance of the controller using the linear stability metrics of the reference model. It is commonly studied to merge indirect and direct methods to guarantee the tracking error reduction and to cancel the uncertainty uniformly which bring about the weight convergence [18], [19]. However, these methods require

persistent excitation of the system for weight convergence. Concurrent learning adaptive law distinguishes from the others with its flexibility on PE condition which is proposed by Chowdhary [17], [20]–[22]. Concurrent learning algorithm uses the recorded data with the current data for adaptation uses a sufficient richness condition on the recorded data to guarantee the weight convergence instead of the restrictive PE condition on the reference input. This condition is more preferable than the PE condition since its requirements are dependent on the spectral properties of the recorded data whereas the PE condition puts restrictions on the future data which is hard to monitor and hard to guarantee.

Adaptive control of guided bombs has been addressed by many studies recently each focused on different aspects of the problem. In addition to stand alone adaptive controller schemes [1], adaptive elements are also used as augmentations to roughly designed baseline controllers. One of many is [2], in which a dynamic inversion based autopilot is upgraded with Model Reference Adaptive Control (MRAC) and L1 adaptive elements. In this study, it is shown that adding an adaptive part to the controller, renders possible to ease the time consuming baseline autopilot design. Also, the suggested L1 element patched autopilot structure is proven to handle the nonlinear dynamic couplings of which the baseline autopilot is incapable to overcome. [3] is another example of MRAC scheme which is used to converge the closed loop response of the plant with unknown coefficients to a desired performance level. Neural network augmentation is another commonly used control architecture which is powerful for estimation of model uncertainties. [4]-[7] present pioneering researches on the application of neural network augmentation to baseline dynamic inversion controllers for air to air missiles, aircraft, tilt-rotor and helicopter. In [8] and [9] an implementation and application of an online learning neural network augmentation to a dynamic inversion based acceleration autopilot of a family of guided munition is given. One of the most famous adaptive control applications of guided munitions was conducted by Boeing Company in 2005. A model reference adaptive controller was implemented to a modified version of Mk-82 Joint Direct Attack Munition (JDAM). An LQR baseline controller is modified with an MRAC

adaptive element to handle the external configuration changes due to the guidance kit addition. The flight tests of JDAM were culminated successful in 2006. The open problems encountered in JDAM flight tests related to the operation of adaptive controller is explained in detail in [10].

1.3 Contributions of This Thesis

In literature, the most common approach to model the uncertainty in adaptive control schemes is to express the uncertainty as a function of the system states. In spite of the fact that any uncertainty shows itself as a disturbance on the system states could be defined by way of the system states, it should also be possible to express the uncertainty as a function of the conclusive origin of the uncertainty. This study states that if the source of the disturbance is apparent and sufficient information related to its dynamics is known, the relation between the plant and the source of the uncertainty could be learned and controlled through appropriate basis functions and concurrent learning adaptive control algorithms. In this research, the roll-pitch coupling of the guided munition which affects the roll stabilization is studied as an example to the claimed statement. The decoupled roll dynamics are stable around the local linearization point, but violation of the linearization conditions such as maneuvers with high angles of attack triggers the dynamic couplings. The unknown and unaccounted relation between the pitch and roll channels is known to arise with pitching maneuvers; hence, the uncertainty is expressed as a function angle of attack rather than a combination of the roll rate (roll channel angular velocity) and the roll angle.

Since the structure of the uncertainty is unknown, the basis function selection should be carefully established. Despite the fact that there exist many wing rock dynamics theories and models in the literature, the phenomenon apparent in this study is not consistent with the well-known definition of the wing-rock notion which refers to limit cycle oscillations in the roll dynamics. A neural network based uncertainty parameterization is not leaned to due to the excessive number of tuning parameters

and the difficulty in weight convergence of commonly used activation functions. The activation functions should span the whole uncertainty domain to make the adaptive weights converge as a necessary, but not sufficient condition, and such construction effort could be troublesome and time consuming. In [23]–[26] Nguyen proposes using Chebyshev polynomials as basis function for a least-squares MRAC scheme. Chebyshev polynomials form a series of orthogonal polynomials which is vital in the theory of approximation. The orthogonality property ensures the linear independency of the polynomial series which contribute to weight convergence and enclosure of the whole uncertainty domain.

Considering all these, in this study, the angle of attack dependent uncertainty is modelled via Chebyshev orthogonal basis functions and the concurrent learning MRAC is used to control and learn the dynamics of pitch-yaw couplings. This thesis proposes a novel uncertainty parameterization method and merges the prominent contributions of different adaptive control studies to enhance and identify roll-pitch couplings of a guided munition.

1.4 Organization of the Thesis

The remainder of the thesis is organized as follows. Chapter 2 includes general missile dynamics derivation for unfamiliar readers. In Chapter 3, linear models are derived and baseline autopilot schemes with linear augmentations are proposed. Chapter 4 addresses the theoretical background of the classical and concurrent learning model reference adaptive controllers. The Chebyshev polynomial basis functions and uncertainty parameterization using disturbance states are covered. The linear model implementations of the studied controllers are also given in Chapter 3 and 4. In Chapter 5, evaluation of the controller performances are conducted through the 6 DoF nonlinear flight simulation in pre-specified flight conditions which simulates the challenging and nonlinear maneuvers. The conclusions and further researches are summarized in Chapter 6. The pitch and yaw channel acceleration

autopilots and their designs are also included in the Appendix A for the integrity of the content.

CHAPTER 2

MISSILE DYNAMICS AND CHARACTERISTICS

In this chapter, equations of motion for a generic missile are derived using Newton's 2nd law of motion for rigid bodies. The structure of the nonlinear aerodynamic database that is used in the high fidelity 6 degree of freedom simulation is introduced; the reference coordinate frames and the dynamical model of the missile are presented.

2.1 Coordinate Systems

In order to describe the motion of the missile, missile body fixed coordinate system and the Earth fixed coordinate system are used. The Earth fixed coordinate system is assumed as the inertial reference frame considering the fact that the missile's motion is much faster than earth's rotation and the missile's range is much shorter than the radius of the earth.

Referring to the Figure XX, (X_e, Y_e, Z_e) denotes the right-handed Earth-fixed coordinate system in which the $X_e, -Y_e$ lie in the horizontal plane and the Z_e -axis points down vertically in the direction of gravity. The body axis system is denoted by (X_b, Y_b, Z_b) is fixed with respect to the missile. The positive X_b -axis coincides with longitudinal axis in forward direction, the positive Z_b -axis points down and Y_b -axis is the complementary right handed axis with respect to X_b and Z_b . The Euler angles (ψ, θ, φ) describes the missile's attitude with respect to the Earth-fixed axes. In Figure XX, the Euler angles and rates are defined whereby the order of rotation of the missile axes is yaw, pitch and roll.

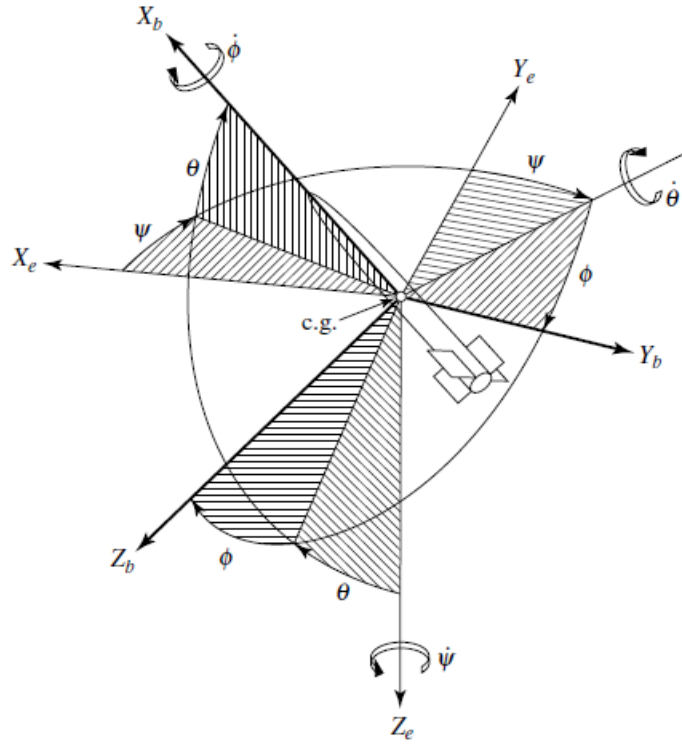


Figure 2.1-1 Orientation of the missile axes with respect to the Earth-fixed axes

The orthogonal transformation matrix from the missile body axes frame to the Earth-fixed coordinate system $C^{(e,b)}$ is achieved by a yaw, pitch and roll rotation about the longitudinal, lateral and normal axes, respectively. The transformation can be written as follows

$$\begin{bmatrix} X_e \\ Y_e \\ Z_e \end{bmatrix} = C^{(e,b)} \begin{bmatrix} X_b \\ Y_b \\ Z_b \end{bmatrix} \quad (2.1)$$

The transformation matrix is defined below where c and s stands for cosine and sine functions.

$$C^{(e,b)} = \begin{bmatrix} c\theta c\psi & s\phi s\theta c\psi - c\phi s\psi & c\phi s\theta c\psi + s\phi s\psi \\ c\theta s\psi & s\phi s\theta s\psi + c\phi c\psi & c\phi s\theta s\psi - s\phi c\psi \\ -s\theta & s\phi c\theta & c\phi c\theta \end{bmatrix} \quad (2.2)$$

It should be noted here that ambiguities (or singularities) can result from using the above transformation (i.e., as $\theta, \phi, \psi \rightarrow 90^\circ$). Therefore, in order to avoid these ambiguities, the ranges of the Euler angles (ϕ, θ, ψ) are limited as follows

$$\begin{aligned} 0 &\leq \phi < 2\pi \\ -\pi &\leq \psi < \pi \\ 0 &\leq \theta \leq 2\pi \end{aligned} \tag{2.3}$$

2.2 Rigid Body Equations of Motion

The assumptions made for deriving the equations of motion are given as follows:

1- The missile is assumed to be a rigid body with a constant mass which does not undergo any change in shape and size.

2- The aerodynamic forces and moments acting on the vehicle are assumed to be invariant with the roll position of the missile relative to the free-stream velocity vector.

3- The missile equations of motion are written in the body-axes coordinate frame and vehicle aerodynamics are nonlinear

Translational and rotational motions of the missile are expressed as follows with the conservation of both linear and angular momentum.

$$\sum \vec{F} = \frac{d}{dt} (m\vec{V}) \Big|_I \tag{2.4}$$

$$\sum \vec{M} = \frac{d\vec{H}}{dt} \Big|_I \tag{2.5}$$

The force equation takes the following form in terms of the body axes

$$\sum \vec{F} = m \left. \frac{d\vec{V}_M}{dt} \right|_B + m(\vec{\omega} \times \vec{V}_M) \quad (2.6)$$

For a missile with $X_b - Z_b$ plane of symmetry, missile's linear equations of motion are expressed in the following scalar form

$$\begin{aligned} F_x &= m\dot{u} + qw - rv \\ F_y &= m\dot{v} + ru - pw \\ F_z &= m\dot{w} + pv - qu \end{aligned} \quad (2.7)$$

where F_x, F_y, F_z are components of the total force acting on the missile expressed in the body frame, including aerodynamic and gravitational forces.

The conservation of the angular momentum is expressed as given below in the body coordinate frame

$$\sum \vec{M} = \left. \frac{d\vec{H}}{dt} \right|_B + \vec{\omega} \times \vec{H} \quad (2.8)$$

where

$$\vec{H} = \sum \vec{r} \times m\vec{V} = \sum m\vec{r} \times (\vec{\omega} \times \vec{r}) \quad (2.9)$$

Using (2.8) and (2.9), the scalar angular momentum equations are obtained as given below

$$\begin{aligned} L &= \dot{p}I_x + (I_z - I_y)qr - (\dot{r} + pq)I_{xz} \\ M &= \dot{q}I_y + (I_x - I_z)pr + (p^2 + q^2)I_{xz} \\ N &= \dot{r}I_z + (I_y - I_x)pq - (\dot{p} - qr)I_{xz} \end{aligned} \quad (2.10)$$

It should be noted that for cruciform missiles with rotational symmetry, $I_z = I_y$ and $I_{xz} = 0$. Also, due to the usual the symmetry of air vehicles about the $X_b - Y_b$ plane, the products of inertia that involve y are usually omitted and the moment equations could be rewritten as follows

$$\begin{aligned} L &= \dot{p}I_x + (I_z - I_y)qr \\ M &= \dot{q}I_y + (I_x - I_z)pr \\ N &= \dot{r}I_z + (I_y - I_x)pq \end{aligned} \quad (2.11)$$

Total velocity and wind angles are calculated as given under no wind assumption

$$V = \sqrt{u^2 + v^2 + w^2} \quad (2.12)$$

$$\alpha = \tan^{-1}\left(\frac{w}{u}\right) \quad (2.13)$$

$$\beta = \tan^{-1}\left(\frac{v}{u}\right) \quad (2.14)$$

2.3 Aerodynamic Forces and Moments

Since guided munitions are missiles with no propulsion unit, the forces acting on the missile could be classified as gravitational and aerodynamic forces. In this section, aerodynamic forces and moments acting on the body are defined, briefly.

$$\bar{F}^B = \begin{bmatrix} F_x \\ F_y \\ F_z \end{bmatrix} = \begin{bmatrix} X + G_x \\ Y + G_y \\ Z + G_z \end{bmatrix} \quad (2.15)$$

The total force acting on the body could be expressed as a column vector written in body axes as given in (2.12). In this expression, X, Y, Z defines aerodynamic forces and G_x, G_y, G_z defines the gravitational forces. The aerodynamic forces are expressed as follows

$$\begin{aligned}
X &= QSC_X \\
Y &= QSC_Y \\
Z &= QSC_Z
\end{aligned} \tag{2.16}$$

where the aerodynamic coefficients are functions of Mach, M , angle of attack, α , and side-slip angle, β , elevation, rudder and aileron deflections, $\delta_e, \delta_r, \delta_a$, and body rates, p, q, r as given below

$$\begin{aligned}
C_X &= f(M, \alpha, \beta, \delta_e, \delta_r) \\
C_Y &= C_{Y_{STATIC}} + C_{Y_{DYNAMIC}} \\
C_Z &= C_{Z_{STATIC}} + C_{Z_{DYNAMIC}}
\end{aligned} \tag{2.17}$$

$$\begin{aligned}
C_{Y_{STATIC}} &= f(M, \alpha, \beta, \delta_r); & C_{Y_{DYNAMIC}} &= f(M, V, r) \\
C_{Z_{STATIC}} &= f(M, \alpha, \beta, \delta_e); & C_{Z_{DYNAMIC}} &= f(M, V, q)
\end{aligned}$$

Aerodynamic moments and moment coefficients are expressed as below with the coefficients calculated at the center of gravity of the missile

$$\begin{aligned}
L &= Qs d C_L \\
M &= Qs d C_M \\
N &= Qs d C_N
\end{aligned} \tag{2.18}$$

$$C_N = C_{N_{STATIC}} + C_{N_{DYNAMIC}} \tag{2.19}$$

$$\begin{aligned}
C_{L_{STATIC}} &= f(M, \alpha, \beta, \delta_a); & C_{L_{DYNAMIC}} &= f(M, V, p) \\
C_{M_{STATIC}} &= f(M, \alpha, \beta, \delta_e); & C_{M_{DYNAMIC}} &= f(M, V, q, \dot{\alpha}) \\
C_{N_{STATIC}} &= f(M, \alpha, \beta, \delta_r); & C_{N_{DYNAMIC}} &= f(M, V, r, \dot{\beta})
\end{aligned}$$

Dynamic pressure, Q , in the equations (2.13) and (2.15) is defined as functions of missile total velocity and air density as given below

$$Q = \frac{1}{2} \rho V^2 \tag{2.20}$$

The air density in the above expression is defined with the following equation

$$\rho(h) = \begin{cases} \rho_0(1 - 0.00002256h)^{4.256} & ; h \leq 10000m \\ 0.412e^{-0.000151(h-10000)} & ; h > 10000m \end{cases} \quad (2.21)$$

2.4 Gravitational Forces

The gravity originated force components are expressed as below in the body frame

$$\bar{G}^B = \begin{bmatrix} G_x \\ G_y \\ G_z \end{bmatrix} = \begin{bmatrix} -mg \sin \theta \\ mg \sin \phi \cos \theta \\ mg \cos \phi \cos \theta \end{bmatrix} \quad (2.22)$$

2.5 Missile Characteristics

In this section, physical parameters and of the missile are given. Physical specifications of the gravity drop bomb Mk-82 is obtained via [27] as follows

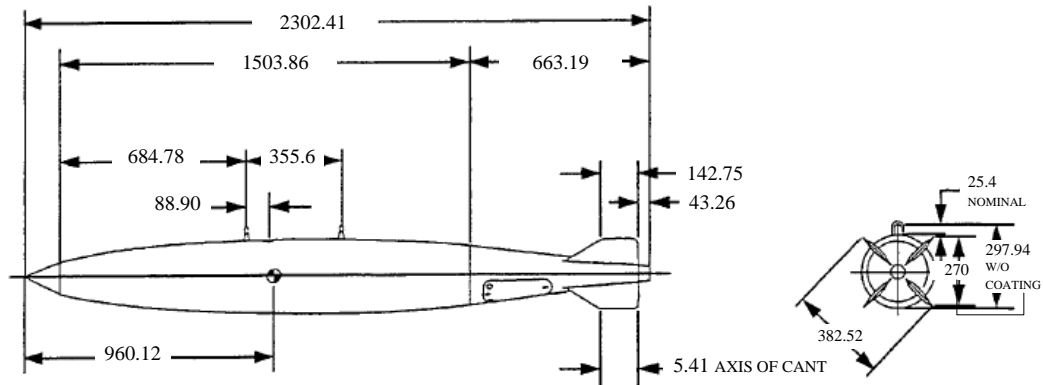


Figure 2.5-1 Layout of Mk-82 General Purpose Low Drag (GPLD) 500 lb bomb (all dimensions in mm)

The physical characteristics of Mk-82 are tabulated in the following table.

Table 2.5-1 Physical characteristics of 500 lb (225 kg) Mk-82 GPLD bomb

Length, assembled	2.30 m
Body diameter	0.27 m
Fin (conical type)	
Span	0.3835 m
Chord	0.2692 m
Weight	10.9 kg
Total Weight (nominal)	240.9 kg
Explosive Weight (nominal)	87.1 kg
Case Weight (nominal)	141.1 kg
Center of Gravity (from nose)	0.96 m
Moments of inertia	
Pitch	49.8 kgm ²
Yaw	49.8 kgm ²
Roll	2 kgm ²

CHAPTER 3

BASELINE ROLL AUTOPILOT AUGMENTATIONS

There has been an increasing demand for greater performance from aerial vehicles which leads to wider flight envelopes with large range of altitudes, speeds and higher angles of attack with rapid changes in aerial platform's aerodynamic characteristics. The technologic developments bring the focus on agile aerial vehicles whereas the industry is steered through cheaper and accessible alternatives. The guided munitions are emerged in response to this need. The gravity bombs which had widely been in use until the second half of World War II are retrofitted with a guidance kit to increase their target hit success while decreasing the collateral damage caused by traditional gravity bombs. These guidance kits usually involve GPS, INS, seeker, fin actuators and some other structural elements to regulate the air flow on the advanced munition. All these additional components enhance the target hit capability of the munition significantly but they bring along some aerodynamic challenges as well. The munition studied in this thesis, tends to undergo dynamic couplings during high angle of attack required manoeuvres. The main consequence of this situation manifests itself with the difficulties in stabilization of the roll channel. The decoupled aerodynamics assumption which is put forward during linear controller design holds any longer and the induced roll angle aggravates the command tracking performance of pitch autopilot. This study briefly focuses on the stabilization of roll channel under cross-coupled interactions by means of augmentations on the roll autopilot. In this chapter, baseline augmentations are commented and the work is extended to adaptive control algorithms in the next chapter.

3.1 Cascaded Roll Autopilot Design

The roll channel controller is a cascaded two-loop regulator as given in Figure 3.1-1 with proportional control.

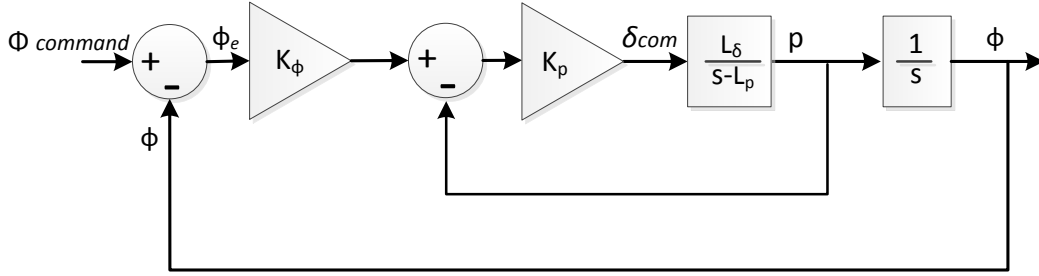


Figure 3.1-1 The baseline roll autopilot structure

Baseline roll channel control law is defined in (3.1)

$$\delta_{bl} = (\phi_e \cdot K_\phi - p) \cdot K_p \quad (3.1)$$

The gain selection procedure is similar to the one given for the acceleration autopilots design. Since the order of the system is reduced by eliminating control actuation system states δ and $\dot{\delta}$ in the feedback, the parametric transfer function of the closed loop system could be obtained easily as follows

$$G_{CL}(s) = \frac{K_\phi K_p L_\delta}{s^2 + (K_p L_\delta - L_p)s + K_\phi K_p L_\delta} \Rightarrow \frac{\omega_n^2}{s^2 + 2\zeta\omega_n s + \omega_n^2} \quad (3.2)$$

Using the mathematical relations, the following analytical expressions are attained for the gains K_ϕ and K_p

$$K_p = \frac{2\zeta\omega_n + L_p}{L_\delta} \quad (3.3)$$

$$K_\phi = \frac{\omega_n^2}{2\zeta\omega_n + L_p} \quad (3.4)$$

By setting the desired damping ratio as $\zeta = 1$, the gains become the function of desired natural frequency only. The desired response of the roll autopilot is defined as being able to reset 10° roll angle ϕ with adequate transient response characteristics. This should not be interpreted as the failure of the roll autopilot at higher roll angles. It must be noted that this is a design approach. The autopilot resets the error and provides the $0^\circ \phi$ condition ultimately in nominal cases by means of the implicit integrator of roll dynamics. In real life applications, the autopilot commands are limited in order not to saturate the control authority suddenly. The autopilot operates only knowing the amount of the error that is being commanded at a time instant which makes the mentioned design approach reasonable.

3.2 Roll Autopilot Augmentation with Feedforward Controller

The initial approach to control the munition is to control acceleration on pitch and yaw channels via full state feedback control law and to use cascaded two-loop autopilot to regulate roll dynamics. The design of pitch and yaw acceleration autopilots are included in Appendix A for the integrity of the context. Acceleration commands on pitch and yaw channels induce a rolling moment and roll angle on the missile due to dominant pitch-roll and yaw-roll coupling characteristics and the cascaded roll autopilot remains incapable to suppress this induced rolling motion. The first idea to enhance the roll stabilization comes up with the analysis of roll aerodynamics. The roll moment coefficient variation with angle of attack for a chosen Mach point at different angles of attack and fin deflections are given in Figure 3.2-1 and Figure 3.2-2

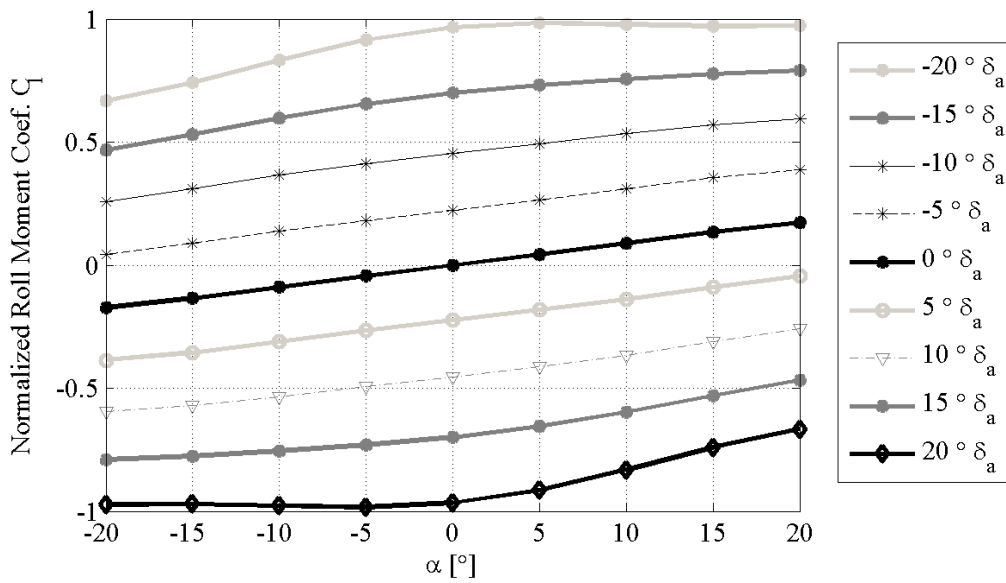


Figure 3.2-1 Variation of Roll Moment Coefficient with α at $0^\circ \beta$

It could be interpreted from Figure 3.2-1 that the variation of roll coefficient with angle of attack is linear at $0^\circ \beta$ for different fin deflections. Figure 3.2-2 shows that the linear variation of C_1 with α is highly dependent on β . At side slip angles greater than 10° , the linear dependency of C_1 on α is limited with $\pm 5^\circ \alpha$

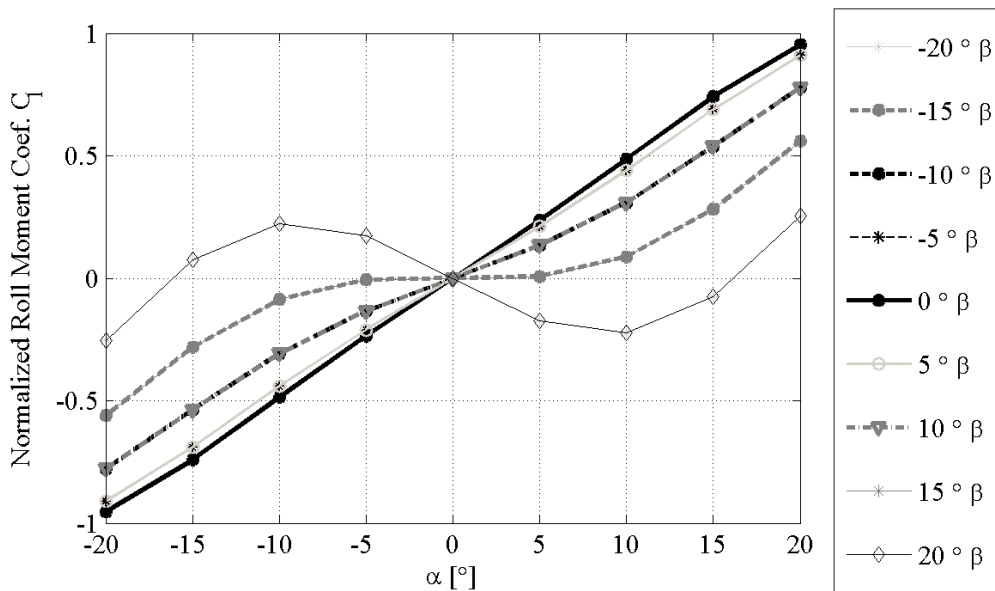


Figure 3.2-2 Variation of Roll Moment Coefficient with α at $0 \delta_a$

In the view of such information, it is concluded that on a limited operation envelope, it is possible to express the variation of roll coefficient with angle of attack linearly. Hence the linear expression for roll dynamics is expanded with a term that defines the rolling moment contribution of angle of attack. The aim of the C_l vs α curve at $0^\circ \beta$ and $0^\circ \delta_a$ defines an additional aerodynamic coefficient which is denoted with C_{l_α} in this study. The rolling moment contribution of angle of attack is calculated like the other static aerodynamic derivatives.

$$L_\alpha = Q \cdot S \cdot C_{l_\alpha} \quad (3.5)$$

$$L = \dot{p} \cdot I_x = L_p \cdot p + L_{\delta_a} \cdot \delta_a + L_\alpha \cdot \alpha \quad (3.6)$$

At this point, the main aim is to obtain a relation between the angle of attack and the roll rate p . The transfer functions derived from equation (3.6) are given in equation (3.7)

$$\frac{p}{\delta_a} = \frac{L_{\delta_a} / I_x}{s - L_p / I_x} \quad \frac{p}{\alpha} = \frac{L_\alpha / I_x}{s - L_p / I_x} \quad (3.7)$$

The angle of attack induced roll moment is defined with the linear variation of roll rate with α . Starting from this, the control strategy is developed leaning on the following logic: Any maneuver which requires angle of attack, induces an amount of roll rate on the missile which is defined with p/α transfer function and the necessary aileron deflection to overcome an amount of roll rate is known via p/δ_a transfer function. Based on these facts, one could build a linear relation between the angle of attack and the aileron deflection. Hence, the necessary additional control effort which compensates the induced roll rate could be calculated.

$$\frac{\delta_a}{\alpha} = \frac{p}{\alpha} \cdot \left(\frac{p}{\delta_a} \right)^{-1} = \frac{s \cdot L_{\alpha} / I_X - \left(L_p L_{\alpha} / I_X^2 \right)}{s \cdot L_{\delta_a} / I_X - \left(L_{\delta_a} L_p / I_X^2 \right)} \quad (3.8)$$

The low frequency gain of the above biproper transfer function is the ratio between the angle of attack on the missile and the necessary aileron deflection which overcomes the roll moment induced due to this angle of attack. Hence, the low frequency gain of this transfer function is assigned as a feedforward control gain K_{ff} on angle of attack and the control law is updated as shown in equation (3.9)

$$\delta_{com} = \delta_{bl} + \delta_{ind} \quad (3.9)$$

where the baseline control input δ_{bl} and the induced control input δ_{ind} are defined as

$$\begin{aligned} \delta_{ind} &= \alpha \cdot K_{ff} \\ \delta_{bl} &= (\phi_e \cdot K_{\phi} - p) \cdot K_p \end{aligned} \quad (3.10)$$

The controller is tested in linear model where the alpha induced roll moment is also included using the transfer functions in equation (3.7). Linear model with feedforward augmented controller is given below. The control actuation system is assumed to be perfect and included as unity in the linear analysis.

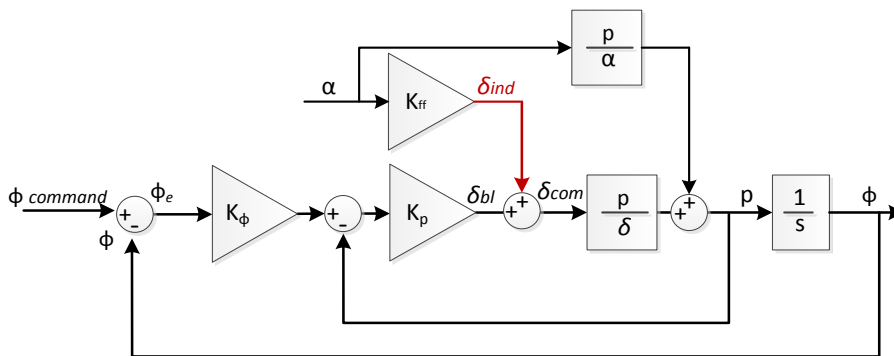


Figure 3.2-3 The linear test model for roll autopilot

In order to include the effect of angle of attack in linear roll dynamics, the related transfer function is taken into the loop as shown. An angle of attack profile which is

1 Hz square wave with 10° amplitude and 2° offset is introduced to the test model. The initial conditions are arranged as $[\phi_0 \ p_0]^T = [10^\circ \ 0]$ and the controller is expected to set the states to zero. The responses of linear model with and without feedforward controller are shown in Figure 3.2-4 and Figure 3.2-5

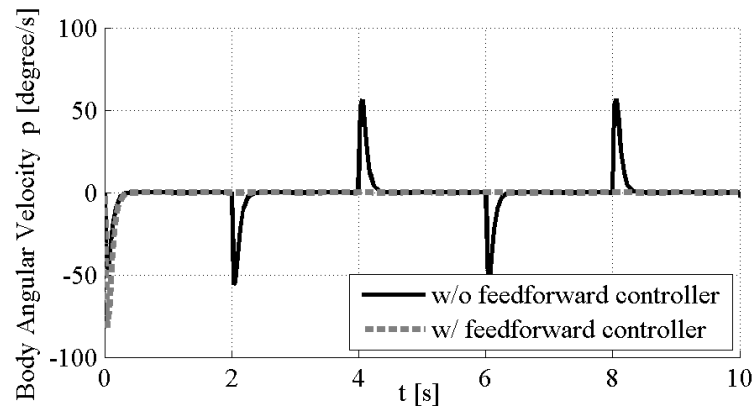


Figure 3.2-4 Linear Simulation Roll Rate Responses of the Cascaded Roll Autopilot with and without Feedforward Controller

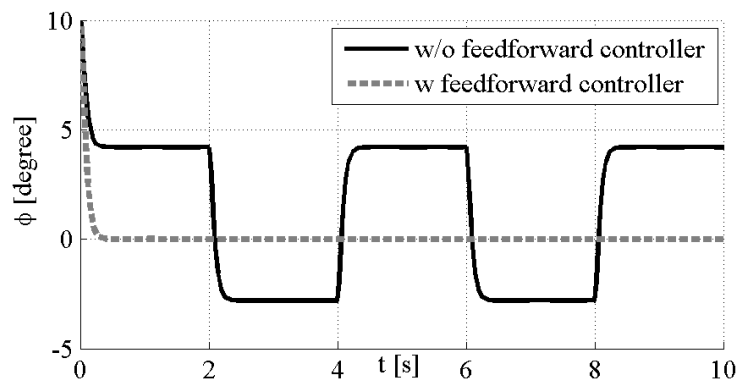


Figure 3.2-5 Linear Simulation Roll Angle Responses of the Cascaded Roll Autopilot with and without Feedforward Controller

The body angular velocity around x-axes, p , and the roll angle ϕ responses show that the induced roll moment due to angle of attack could be eliminated in linear space

with feedforward control signal. The problem with this control strategy is that it is based on the linear relation between angle of attack and roll rate. This linear relation only holds true between the linear region limits of the aerodynamic database which is roughly $\pm 5^\circ$ angle of attack, side slip angle and fin deflection angle. The other point to consider is the effect of the aerodynamic uncertainties to the feedforward control scheme. The robustness performance of the controller should be assessed by taking the uncertainty tolerances of the database into account. Also, it must be emphasized that the studied munition is not symmetric and has different aerodynamical characteristics in pitch and yaw channels. Hence, the linear relation constituted between angle of attack and roll rate could not be established between side slip angle and roll rate. Nonlinear application of the feedforward controller and its further drawbacks are discussed in Chapter 4.

3.3 Fixed Gain Model Reference Controller Design for Roll Channel

The cascaded roll autopilot remains incapable to suppress the induced rolling motion from dominant coupling characteristics and the feedforward control scheme is only applicable to a small region which is limited by linear α - C_l interaction envelope. To eliminate this phenomenon, a fixed gain model reference controller is designed as explained in this section. This concept aims to match the system asymptotically with the desired reference model behaviour. The control law forces the system to imitate the reference model responses where the reference model is chosen such as:

$$\dot{x}_{rm}(t) = A_{rm}x_{rm}(t) + B_{rm}r(t) \quad (3.11)$$

The reference model in our case is driven by the commanded roll angle and produces the reference roll rate and the reference roll angle. The system is assumed to be modelled perfectly

$$\dot{x}(t) = Ax(t) + Bu(t) \quad (3.12)$$

The error which is intended to be eliminated is expressed as

$$e(t) = x_{rm}(t) - x(t) \quad (3.13)$$

A feedback-feedforward control law is defined in (3.14)

$$u(t) = K_{pd}e(t) + K_{ff}x_{rm}(t)^T + K_r r(t) \quad (3.14)$$

The error dynamics is derived as given below

$$\dot{e}(t) = \dot{x}_{rm}(t) - \dot{x}(t) \quad (3.15)$$

$$\dot{e}(t) = A_{rm}x_{rm}(t) + B_{rm}r(t) - (Ax(t) + B(u(t) + \Delta(x))) \quad (3.16)$$

Inserting equation (3.13) and (3.14) into (3.16) and gives the following where $\Delta A = A_{rm} - A$

$$\dot{e}(t) = \Delta Ax_{rm}(t) + B_{rm}r(t) + Ae(t) - BK_{pd}e(t) - BK_{ff}x_{rm}(t) - BK_r r(t) \quad (3.17)$$

The matching condition states that

$$\Delta Ax_{rm}(t) + B_{rm}r(t) = BK_{ff}x_{rm}(t) + BK_r r(t) \quad (3.18)$$

which leads to the following relations

$$\begin{aligned} A_{rm} &= A + BK_{ff} \\ B_{rm} &= BK_r \end{aligned} \quad (3.19)$$

The error dynamics is simplified as given in (3.20)

$$\dot{e}(t) = (A - BK_{pd})e(t) \quad (3.20)$$

Using error feedback instead of state feedback in fixed gain model reference controller allows designer to obtain any desired transient response while tracking a given reference command. The structure of MRC and the linear model responses under the presence of angle of attack presence are given as follows.

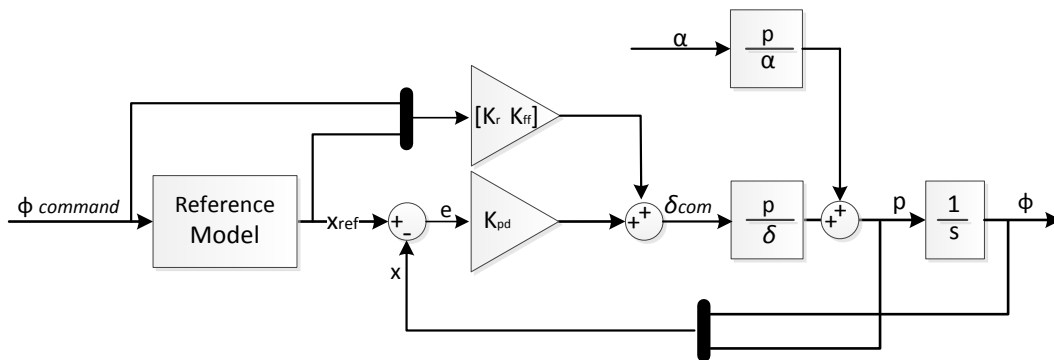


Figure 3.3-1 Model Reference Controller Structure

It should be noted that the plant could be easily modified to let the angle of attack originated disturbance enter the system through the control channel which defines it as a matched disturbance.

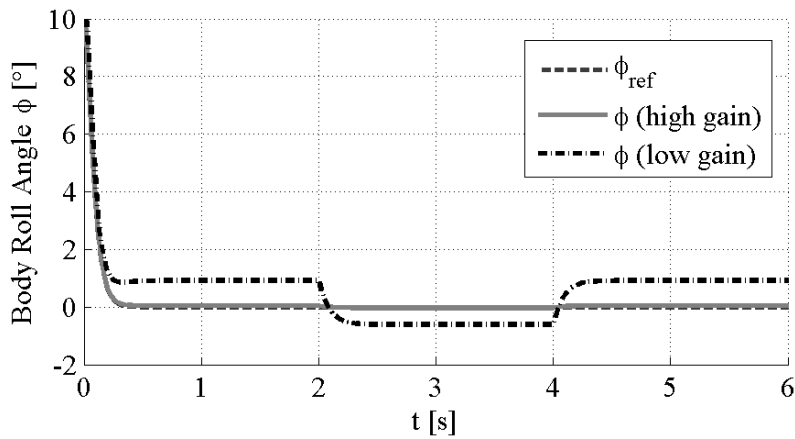


Figure 3.3-2 Linear Simulation Roll Angle Responses of Model Reference Controller

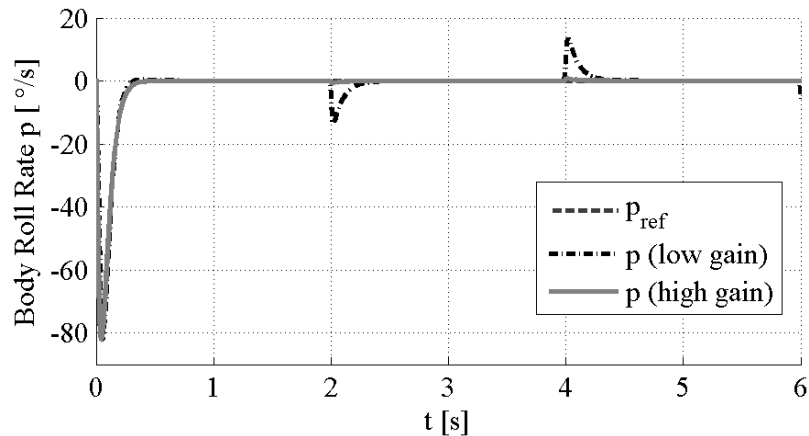


Figure 3.3-3 Linear Simulation Roll Rate Responses of Model Reference Controller

In the above example, the nominal closed loop model of the cascaded roll autopilot is used as a reference model. The plant is at 10° roll angle initially and the MRC is able to stabilize the states which are disturbed by induced roll rate due to angle of attack. MRC is applied with a high and a low error feedback gain and both of the two configurations are able to track the reference model adequately in nominal case. The low gain configuration underperforms in disturbed case whereas the high gain configuration still performs well. However, the simulation step size is needed to be reduced about a 1000 times to prevent the divergence of high gain configuration which brings about a computational load and usually restricted with practical limitations in real applications. Another and the most important issue of MRC is the ideal plant assumption which is rarely the case in real world. Parametric uncertainties could lead to instabilization of the plant; even if the plant stays stable, the closed loop performance of the system could degrade to a level beyond the admissible limits.

CHAPTER 4

ADAPTIVE ROLL AUTOPILOT DESIGN

In the previous chapter, the system dynamics is assumed to be known completely, which is hardly the case in reality. The aerodynamic parameters are rarely known exactly and this type of uncertainty is called the parametric uncertainty. The controllers as such in the previous chapter could lead to deterioration of the closed loop performance and even instabilities if the parameters are drastically distinct from their true values. This situation emerges an inspiration for using adaptive gain adjustment mechanisms. The baseline autopilots are controllers with limited flight envelope coverage and adaptive augmentation is expected to adjust the baseline control inputs appropriately to guarantee the expected performance even under off-design conditions. The adaptive control theory gained popularity in the early 1950s to cover the control expectations of agile aircrafts and the concept of model reference adaptive systems (MRAS) was suggested soon in 1958 by Whitaker et al. at MIT [2]. The idea was to dictate the desired servo-tracking performance using a difference equation (reference model). This control concept is now called as explicit model following and the related controller scheme is known as the model reference adaptive control (MRAC). In this chapter, firstly a model reference adaptive controller (MRAC) is designed for roll channel, and then the MRAC is augmented with a concurrent learning algorithm as in [17], [28].

4.1 Why Adaptive Control?

The need for using adaptive schemes arises in view of the following few issues. The most prominent reason is the uncertainties in the database considering that to put an aerodynamic database into a final form is a long process. The initial versions of a database usually do not include the protrusions around the main body such as the GPS antenna or the external wireway between the seeker and the actuator. Hence, the database does not necessarily reflect the undesired aerodynamic effects of these asymmetric structural elements. In addition, computational studies are generally conducted for limited design conditions and might not reveal the whole story behind any possible problematic phenomena. Besides, the structural design usually goes under improvements with the evolving operational needs as the project proceeds. Despite all these, the controller design task should be conducted up to a level relying on the available information provided with the database and the adequate robustness should be introduced to lower the labour of fine tuning with any design update. Using an adaptive controller scheme contributes to enhance all of these mentioned issues. Adaptive schemes introduce robustness against the parametric uncertainties and reduce the development costs and schedule by eliminating the need for expensive wind tunnel testing. Also, the studied guidance kit is designed to be compatible with a family of iron bombs with various mass properties and aerodynamic characteristics hence a self-adaptive controller becomes a must to ensure adequate control capability over a wide range of configurations.

4.2 Uncertainty Parameterization Independent of the System States

The punchline of a superior control is directly related to having a plant model which adequately captures the actual physical system. However, the model simplifications and idealized assumptions usually rule out the nonlinear, coupled and time varying system dynamics. The uncertainties that come naturally with the real life applications such as measurement noise and environmental disturbances (ea. turbulence) together

with the model simplifications could lead to excluding important physical characteristics from the mathematical model. The unknown effects of these ignored dynamics are usually included as an uncertainty term in the model and either a robust control scheme is employed to maintain consistent performance in the presence of uncertainty or an additional control effort is set aside to identify and cancel this uncertainty in the model by means of adaptive controllers.

The uncertainties could be structured or unstructured depending on whether they could be linearly parameterized using a set of known basis functions. If the MRAC is designed to cancel the structured uncertainties, the adaptive element is formed by using this known basis. Parametric uncertainties are included in this class. When the structure of the uncertainty is unknown, but it is defined over a compact domain and continuous; the uncertainty could be approximated up to certain level with Neural Networks or other well-known regression techniques such as polynomial approximation.

The well accepted way to define an uncertainty, either structured or unstructured, expresses the uncertainty as a function of the system states.

$$\Delta(x(t)) = W^*{}^T f(x(t)) \quad (4.1)$$

where W^* denotes a constant unknown gain matrix and $f(x(t))$ denotes the structure of the uncertainty.

In literature, many examples could be found for this type of uncertainty modelling [29], [30]. Despite the fact that any uncertainty that is apparent on the states as disturbance could be modelled through the system states; it should also be possible to include the uncertainty through its directly related variable if there is one. The idea offered in this study is to relax the assumption of the state dependent uncertainty. Defining the uncertainty with its' conducive parameter is expected to contribute especially in identifying the unstructured uncertainties. Even though the structure of the uncertainty is unknown, usually the phenomenon inducing the uncertainty is

conspicuous but it might not be expressed well with system states as happened so in this study.

The main motivation to switch to an adaptive gain update algorithm is to prevent the induced roll motion due to tightly coupled dynamics. The uncertainty dealt with in this study is a modelling error which makes the induced rolling motion unobservable in linear model but it becomes apparent in nonlinear simulation with the presence of angle of attack. Since the main source of the uncertainty is addressed as α ; the uncertainty is modelled as a function it throughout this study.

$$\Delta(\zeta(t)) = W^{*T} f(\zeta(t)) \quad (4.2)$$

where $\zeta(t)$ is called the uncertainty state and it is either α or β or a function of α and β depending on the case. In spite of the fact that the uncertainty is assumed to be independent of the system states, the matched uncertainty assumption still holds, which means that the uncertainty enters the system through the control channel. The advantages and disadvantages of system states independent uncertainty modelling are discussed further in the following chapter.

4.3 Model Reference Adaptive Controller Design for Roll Channel

In the previous chapter, it is stated that the cascaded roll autopilot remains incapable to suppress the induced rolling motion from dominant coupling characteristics and the feedforward control scheme is only applicable to a small region which is limited by linear α - C_l interaction envelope. The MRC assumes the plant is known exactly which makes it sensitive to the parametric uncertainties. This problem reveals a motivation for integrating adaptive controllers to the system as a part of the solution.

To make the roll channel adaptive against the coupled dynamics, the MRC scheme is augmented with an adaptive element. The adaptive controllers are mainly classified as direct and indirect adaptive schemes. The direct adaptive schemes adapt controller in response to system variations whereas indirect control schemes require an

estimation algorithm, estimate the unknown parameters then adapts the controller according to that estimation. In this study, direct MRAC is employed which is highly popular in the control of uncertain systems.

In direct MRAC, the overall plant is modelled as a combination of a nominal (known) part and an unknown part. A reference model is chosen as in MRC which specifies the desired behavior of the closed loop system. The control strategy consists of two parts like the plant: first part is the nominal control which is designed by only considering the known part of the plant. The second part is the adaptive control which is driven by the error between the reference model and the true plant. When there is no uncertainty the adaptive control mechanism does not contribute to the control signal. In the presence of uncertainties, adaptive control provides additional feedback to drive error to zero asymptotically.

Many examples to applications of MRAC could be found in the literature [4], [25], [31]. In view of the related studies, the control law for MRAC roll autopilot is presented in this section. First, the system with matched uncertainty is defined as follows.

$$\dot{x}(t) = Ax(t) + B(u(t) + \Delta(\zeta(t))) \quad (4.3)$$

where $\Delta(\zeta)$ denotes a scalar uncertainty which is a continuous function of the uncertainty states and the pair (A, B) is assumed to be controllable. The term “matched” implies that the uncertainty enters the system where the control input is applied. The matching condition suggests that the controller would be able to cancel the system uncertainties if the uncertainties are known and the matched uncertainty assumption assures existence of at least one control solution. A reference model is designed which forces the plant to perform the desired closed loop response.

$$\dot{x}_m(t) = A_m x_m(t) + B_m r(t) \quad (4.4)$$

where $r(t)$ is bounded reference signal and the system matrix is Hurwitz. The control law is constituted in equation (4.5) where u_e is the error feedback control signal, u_{rm} is the feedforward part and u_{ad} is the adaptive part.

$$u(t) = u_e(t) + u_{rm}(t) - u_{ad}(t) \quad (4.5)$$

The feedback and feedforward control signals are defined in equation (4.6) and the adaptive part is derived in the following sections.

$$\begin{aligned} u_e(t) &= K_{pd}(x_{rm}(t) - x(t)) \\ u_{rm}(t) &= K_r r(t) + K_{ff} x_{rm}(t) \end{aligned} \quad (4.6)$$

4.3.1 Tracking Error Dynamics

In order to define the adaptive control signal, tracking error dynamics is derived based on the error definition given in (4.7)

$$e(t) = x_{rm}(t) - x(t) \quad (4.7)$$

Differentiating (4.7) gives the following

$$\dot{e}(t) = A_{rm} x_{rm}(t) + B_{rm} r(t) - (Ax(t) + B(u(t) + \Delta(\zeta))) \quad (4.8)$$

Equations (4.5) and (4.6) are substituted in (4.8) which results in:

$$\dot{e}(t) = A_{rm} x_{rm}(t) + B_{rm} r(t) - Ax(t) - B(u_{rm}(t) + K_{pd}e(t) - u_{ad}(t) + \Delta(\zeta)) \quad (4.9)$$

At this point, to make the error visible in the above equation the following expressions are defined, $A_{cl} = A - BK_{pd}$ and $\Delta A = A_{rm} - A_{cl}$

$$\dot{e}(t) = \Delta A x_{rm}(t) + B_{rm} r(t) + A_{cl} e(t) - B(u_{rm}(t) - u_{ad}(t) + \Delta(\zeta)) \quad (4.10)$$

A matching condition is assumed to exist such that $Bu_{m}(t) = \Delta Ax_{m}(t) + B_{m}r(t)$. The feedforward control signal is designed considering this condition. Hence, equation (4.10) is simplified as follows:

$$\dot{e}(t) = A_{cl}e(t) + B(u_{ad}(t) - \Delta(\zeta)) \quad (4.11)$$

The cascaded controller gain K_{pd} should be selected such that $A_{cl} = A - BK_{pd}$ is Hurwitz to guarantee the existence of a solution P for the following Lyapunov equation for any positive definite Q

$$A_{cl}^T P + PA_{cl} + Q = 0 \quad (4.12)$$

4.3.2 Adaptive Controller Design

4.3.2.1 Case I: Structured Uncertainty

Adaptive elements in MRAC are divided into two: one of which is designed to cancel the structured uncertainties and the other of which is designed to cancel the unstructured uncertainties. The structured uncertainty means that the uncertainty could be linearly parameterized using a set of nonlinear basis functions. Using this information, the adaptive control signal is generated with a weighted combination of the known basis. Wing rock dynamics is the commonly known member of this type of uncertainty and is widely included in the literature [32]–[38]. In this section, the adaptive controller input u_{ad} is designed to cancel the structured and matched uncertainty $\Delta(\zeta)$. The uncertainty assumption is going to be relaxed and elevated for the unstructured case in the following section.

The uncertainty $\Delta(x)$ is linearly parameterized and it is assumed that there exists a unique constant vector $W^* \in R^m$ and a vector of continuously differentiable and

bounded known regressor functions $\Phi(\zeta(t)) = [\Phi_1(\zeta(t)), \Phi_2(\zeta(t)), \dots, \Phi_m(\zeta(t))]$, such that, an interval $[t, t + \Delta t], \Delta t \in \mathbb{R}^+$ exists over which $\int_t^{t+\Delta t} \Phi(\zeta(t))\Phi^T(\zeta(t))dt$ is positive definite. Then, the uncertainty is uniquely expressed as:

$$\Delta(\zeta(t)) = W^{*T} \Phi(\zeta(t)) \quad (4.13)$$

Letting $W(t) \in \mathbb{R}^m$ denote a good estimate of W^* and considering that the mapping between the states and the uncertainty is known, the adaptive control signal that eliminates the uncertainty could be written as

$$u_{ad}(\zeta(t)) = W^T(t) \Phi(\zeta(t)) \quad (4.14)$$

Then by the selection of a globally radially unbounded quadratic Lyapunov function candidate and using the necessary Lemma's as shown in [39] in detail, the following weight update law is obtained.

$$\dot{W} = -\Gamma \Phi(\zeta) e^T P B \quad (4.15)$$

where $\Gamma \in \mathbb{R}^{m \times m}$ is a positive definite learning rate that drives the error to zero asymptotically.

4.3.2.2 Case II: Unstructured Uncertainty

In many physical applications, there is no known exact structure between the input and the output processes. This type of uncertainty is called the unstructured uncertainty and it is assumed that the uncertainty is continuous and defined over a compact domain. If the uncertainty is structured, the apparent basis function candidate is engaged and when the unstructured uncertainty is the point at issue, universal approximators such as radial basis functions or sigmoidal neural networks are employed to parameterize the unfamiliar uncertainty [11]–[15], [40]–[44]

Multilayer Neural Networks (MLNN) are proven to learn any function theoretically. Nonetheless in applications, it could be challenging to generate a net covering the entire expected uncertainty domain or to provide the sufficient training data. Another issue of the neural networks is the substantial amount of effort to design the network with many parameters needed to be tuned such as number of layers, number of units and activation functions of each unit. Besides the effort in determination of the number of processing elements, neural networks have the problem of local minimum and slow convergence speed which makes them much suitable for long processes [39]

The other common approach to model the unstructured uncertainties is the polynomial approximation. Function approximation using standard polynomials is problematic since the approximation is not guaranteed to converge to the true function independent of the degree of the polynomial. In theory, the degree of polynomial is directly proportional with the precision of the approximation. However, increasing the degree of the approximating polynomial beyond a limit, could cause overparameterization which results in oscillations in the approximated output.

A novel idea is proposed in [24], [25] which elevates the standard polynomial approximation to approximation of the unstructured uncertainty by Chebyshev orthogonal polynomial basis functions. The main advantage of orthogonal functions over a regular polynomial is the better function approximation of orthogonal polynomials than a regular polynomial of the same degree. Orthogonal polynomial basis functions provide a convenient method for approximating functions with a series of linearly independent terms which provide fast convergence and also resolve the local minimum issue in neural networks [24], [25]. In this study, the unstructured uncertainty case is handled using Chebyshev orthogonal polynomials as basis functions considering its superiorities.

4.3.2.2.1 Chebyshev Polynomials

Chebyshev polynomials form a series of orthogonal polynomials which has an important role in the theory of approximation. The polynomials are defined in the following manner for the variable $x \in [-1, 1]$

$$\begin{aligned} T_0(x) &= 1 \\ T_1(x) &= x \\ T_2(x) &= 2x^2 - 1 \\ T_3(x) &= 4x^3 - 3x \\ &\vdots \end{aligned} \tag{4.16}$$

The explicit formula for Chebyshev polynomials is defined as

$$T_n(x) = \cos(n \arccos(x)) \tag{4.17}$$

The polynomials also could be generated using the following recurrence relation for $n \geq 1$:

$$T_{n+1} = 2xT_n - T_{n-1} \tag{4.18}$$

The orthogonality property of these polynomials is defined within the interval $x \in [-1, 1]$ with a weight of $\sqrt{(1-x^2)^{-1}}$ i.e.

$$\int_{-1}^1 \frac{T_i(x)T_j(x)}{\sqrt{1-x^2}} dx = \begin{cases} 0 & i \neq j \\ \pi/2 & i = j \neq 0 \\ \pi & i = j = 0 \end{cases} \tag{4.19}$$

The good thing about the orthogonality property is that a set of orthogonal vectors is guaranteed to be linearly independent while spanning the uncertainty space. This is the reason for the fast convergence of orthogonal basis polynomials with relatively less terms than regular polynomials.

An arbitrary function $F(s)$ can be approximated as follows using Chebyshev polynomials expansion

$$F(s) = \sum_{i=1}^N c_i T_{i-1}(x) \quad (4.20)$$

where T_i are the Chebyshev polynomials, c_i the coefficients of expansion, N the degree of the polynomials and x is a non-dimensional variable defined as

$$x = \frac{2s - (s_{up} + s_{lo})}{s_{up} - s_{lo}} \quad (4.21)$$

s_{up} and s_{lo} are the lower and upper bounds defining the range over which the approximation is valid [45].

4.3.2.2 Unstructured Uncertainty Modelling Using Chebyshev Polynomials

The unstructured uncertainty is approximated using the Chebyshev polynomials expansion in (4.20). The uncertainty which is an unknown function is expressed as:

$$\Delta(\zeta) = f(\zeta(t)) \quad (4.22)$$

It is assumed that the function $f(\zeta(t))$ could be approximated with Chebyshev expansion with N sufficient polynomial terms as follows:

$$f(\zeta) = \sum_{i=1}^N w_i \Phi_i(\bar{\zeta}) \quad (4.23)$$

where $\bar{\zeta}$ is the normalized uncertainty state, $\Phi_i(\bar{\zeta}) = T_{i-1}(\bar{\zeta})$ and $\Phi = [\Phi_1 \ \Phi_2 \ \dots \ \Phi_N]$ is the basis function which is an array of Chebyshev polynomials up to degree $N-1$. $W = [w_1 \ w_2 \ \dots \ w_N]$ denotes the coefficients of Chebyshev polynomial terms and updated with the following weight update rule as in the structured uncertainty case.

$$\dot{W} = -\Gamma \Phi(\bar{\zeta}) e^T P B \quad (4.24)$$

The designed MRAC is tested in linear simulation for structured and unstructured uncertainties. The disturbance is selected as a function of α which is obtained via p/α transfer function.

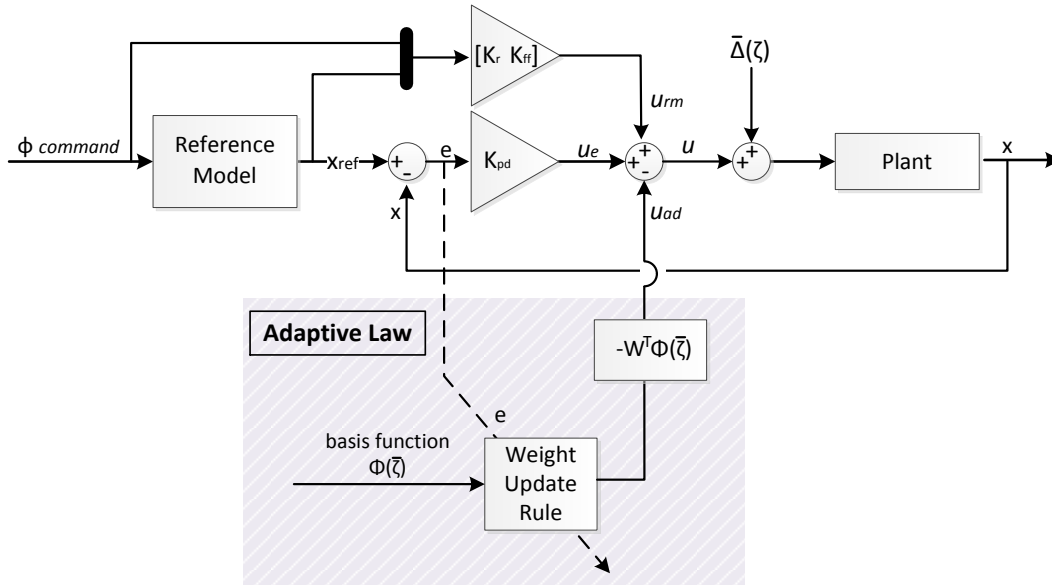


Figure 4.3-1 Model Reference Adaptive Controller Structure

A system with uncertainties is written in the following form:

$$\dot{x}(t) = Ax(t) + Bu(t) + \Delta(\zeta) \quad (4.25)$$

The uncertainty is defined as matched uncertainty if it is possible to express the uncertainty as

$$\Delta(\zeta) = B \cdot \bar{\Delta}(\zeta) \quad (4.26)$$

$$\dot{x}(t) = Ax(t) + B[u(t) + \bar{\Delta}(\zeta)] \quad (4.27)$$

To include disturbance induced with α as a matched uncertainty in the system, the state space model is updated as given below

$$\begin{bmatrix} \dot{\phi} \\ \dot{p} \end{bmatrix} = \begin{bmatrix} 0 & 1 \\ 0 & L_p \end{bmatrix} \begin{bmatrix} \phi \\ p \end{bmatrix} + \begin{bmatrix} 0 \\ L_\delta \end{bmatrix} \left(\delta + \frac{L_\alpha}{L_\delta} \alpha \right) \quad (4.28)$$

The basis function is constructed using the first 4 terms of the Chebyshev expansion. The responses of MRAC for linear system are given in the following figure.

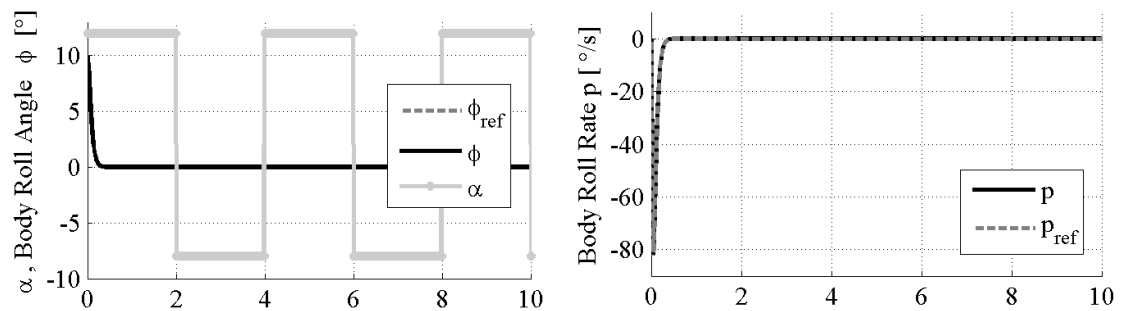


Figure 4.3-2 Linear Simulation Roll Angle, Roll Rate and the Angle of Attack Responses of the MRAC

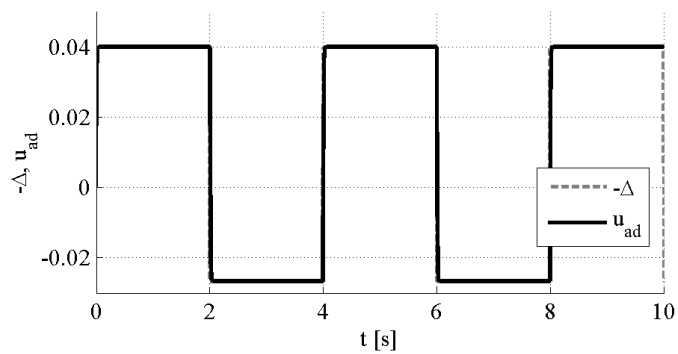


Figure 4.3-3 Structured Uncertainty and the Adaptive Control Input Histories

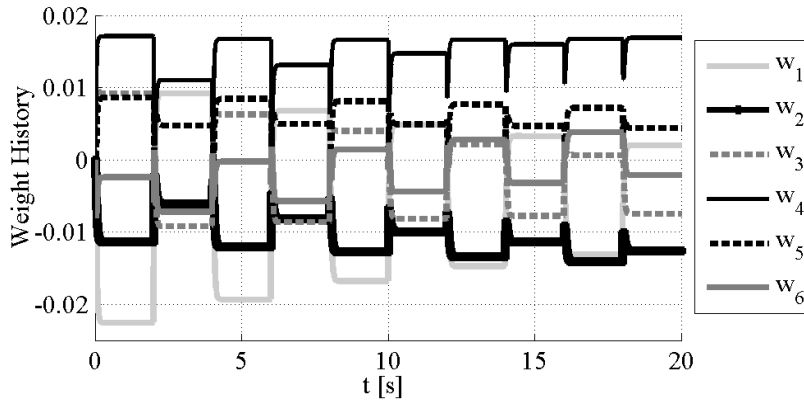


Figure 4.3-4 Adaptive Weight Histories of the MRAC

Figure 4.3-2 shows that the body roll rate and the body roll angle could easily be driven to zero from initial 10° roll angle under the presence of angle of attack. The adaptive control signal and the uncertainty with opposite sign are shown in Figure 4.3-3. It is seen that the adaptive control signal cancels the uncertainty out completely with Chebyshev polynomial basis function. However, the weight history shows that weights do not converge despite the persistently excited reference signal.

Stated by the theory, the interest of MRAC is the asymptotic command tracking and it is achieved despite the system uncertainties. The controllers may yield transient oscillations due to higher adaption rates and weights may not resemble to the actual values. The error that driven asymptotically to zero does not imply the estimation of weights converge to their ideal unknown values. However, in some cases the convergence might come along with the desired tracking. A necessary condition for parameter convergence is the persistency of excitation (PE) which dictates hard to achieve restrictions on the reference signal. For linear systems, PE condition is satisfied if the reference signal is a sum of sinusoids with different frequencies [2]. But in nonlinear systems, this rule no longer holds and verifying the PE conditions become harder numerically. The unobtainable PE condition not only affects the parameter convergence, also risks the boundedness of the adaptive weights. In spite of the fact that there exist some modification methods to guarantee boundedness,

they could cause the weights to stick around their initial guesses due to redundant stiffness on the adaptive law. In order to avoid these problems, PE condition is relaxed by augmentation of classical MRAC scheme with concurrent learning algorithm which is declared by Chowdhary in [39].

4.4 Concurrent Learning Model Reference Adaptive Control

The solution offered in the previous section mainly focuses on finding the instantaneous solution for the control problem with classical MRAC scheme. This scheme ensures generating an appropriate control input at every time instant to cancel the disturbance, however there is no guarantee about the weight convergence which indicates that the algorithm learns the existing disturbance and imitates this learned disturbance to generate the control input. The learning algorithms use the past information to generate a more effective control action iteratively which ultimately improves the tracking accuracy. There are several algorithms to force the online adaptive control schemes to learn the disturbance and some of them are commonly studied in the literature [46]–[52]. The learning algorithm preferred in this thesis is concurrent learning algorithm that is studied by Chowdhary. Concurrent learning algorithm uses the past and present data together to adapt the control law weights. The main benefit of this algorithm is that if the recorded data is rich enough in terms of expressing the disturbance, the weights converge to their true values without the necessity of PE condition. The weight convergence is desirable since it ensures guaranteed exponentially bounded transient performance and exponential error convergence. The convergence of the weights to their true values means that the plant uncertainty is uniformly approximated which makes the tracking error dynamics linear. The linear tracking error dynamics let the plant track the reference model exponentially which indicates that the reference model states and the plant states become indistinguishable at some point if the reference model is properly selected. This situation leads a way through meaningfully evaluating the system in terms of frequency domain specifications and transient characteristics by means of the reference model characteristics. To emphasize the benefits of concurrent learning

algorithm, the PE condition should be defined properly before taking a step further. Boyd and Sastry define the PE condition as follows [31]:

Persistency of Excitation (PE) Condition

A bounded vector signal $\Phi(t)$ is persistently exciting if for all $t > t_0$ there exists $T > 0$ and $\gamma > 0$ such that

$$\int_t^{t+T} \Phi(\tau)\Phi^T(\tau)d\tau \geq \gamma I \tag{4.29}$$

where $\int_t^{t+T} \Phi(\tau)\Phi^T(\tau)d\tau \in R^{m \times m}$.

This condition states that if the exogenous reference input contains as many spectral lines as the number of unknown parameters, then the plant states are persistently excited. In order to remove the PE restriction on the weight convergence using the recorded data, there is still one condition to satisfy on the data stack which is the ‘sufficient richness’. This condition is characterized by the following rule of thumb in [39].

Weight Convergence Condition (WCC)

The history stack should contain as many linearly independent elements $\Phi_k \in R^m$ as the dimension of the basis of the uncertainty. If the history stack is denoted as $Z = [\Phi_1 \ \Phi_2 \ \dots \ \Phi_p]$, the rank condition should be satisfied that $rank(Z) = m$.

The weight convergence condition (WCC) ensures that the history stack is sufficiently rich to form an appropriate basis for the linearly parameterized uncertainty.

The main superiority of WCC to PE condition is the ease of practical application. It is straight forward to determine the rank of a matrix online whereas PE condition is

hard to verify in most cases. For linear systems with linear-in-parameter uncertainties, if the exogenous reference command is chosen as a sum of sinusoids with different frequencies, the PE conditions are satisfied. A single frequency gives exponential convergence of two adaptive gains to their corresponding true values.[2]. However, for nonlinear systems this rule no longer holds and generic PE conditions become hard to verify numerically. Furthermore, in most real cases, the exogenous input is not known a-priori and case dependent which makes online assessment of the PE condition almost impossible. Additionally, exciting the states persistently is not desirable in real applications because of obvious drawbacks such as limited fuel or unnecessary stress loads. On the contrary, the WCC could be met within a sufficient time range without any additional excitation effort.

4.4.1 Concurrent Learning Weight Update Law

The concurrent weight update algorithm is based on the idea of adding a data history based augmentation term on the online MRAC weight update law. The selection of data to record is handled in the following sections and in this section it is assumed that the history stack meets the related rank condition. For $j \in \{1, 2, \dots, p\}$ which denotes index of a recorded data point ζ_j and $\Phi(\zeta_j)$ represents the regressor vector evaluated at that point, concurrent learning gradient descent algorithm is expressed as the following

$$\dot{W}(t) = -\Gamma_c \Phi(\zeta(t)) e^T(t) P B - \sum_{j=1}^p \Gamma_x \Phi(\zeta_j) \varepsilon_j(t) \quad (4.30)$$

where $\Gamma > 0$ represents a positive learning rate matrix and $\varepsilon_j(t) = W^T \Phi(\zeta_j) - \Delta(\zeta_j)$ is the difference between the adaptive control input and the modelling uncertainty. For single input case, the modelling error $\Delta(\zeta_j)$ is expressed as

$$\Delta(\zeta_j) = (B^T B)^{-1} B^T [\dot{x}_j - Ax_j - Bu_j] \quad (4.31)$$

In equation (4.31), A, B, u_j, x_j are known and \dot{x}_j is measured or estimated depending on the installed hardware. In this study, it is assumed that measurement for \dot{x}_j is available. The Lyapunov function candidate selection with related stability and convergence proofs for tracking error and parameter error convergence are covered in detail in [39]. It is also stated that adding or removing data does not affect the Lyapunov candidate and tracking error dynamics $e \equiv 0$ and the weight error dynamics $\tilde{W}(t) = W(t) - W^* \equiv 0$ are guaranteed as long as the WCC is satisfied.

4.4.2 Data Selection Algorithm for the History Stack

In the previous sections, it is stated that concurrent learning algorithm ensures weight convergence if the history stack has as many linearly independent elements as the basis of the uncertainty. Hence, the history stack should be filled with carefully selected data to take the spectral features of the stack under control. To meet the rank condition, an algorithm must be employed to prevent the logging of useless data and to record only the data sufficiently different from the last recorded point. If the history stack could be widen infinitely, there would be no need for implementation of such algorithm, however real applications are restricted by hardware capacity limitations. There are several methods mentioned in the literature for elimination of waste data and quantifying the useful points. One of them is cyclic data history algorithm, which records every sufficiently different data until the stack is full and overwrites the oldest data when an upcoming data is labelled as useful after the stack is full. This method is proven to work effectively in some cases [28], [39] but in general, there is no guarantee of satisfying the rank condition with cyclic stack.

The other method is singular value maximizing (SVM) algorithm. The SVM algorithm is based on the fact that the rate of convergence depends on the minimum

eigenvalue λ_{\min} of the symmetric matrix $\Omega = \sum_{j=1}^p \Phi_j \Phi_j^T$ which has a detailed proof in [28]. Depending on that, the data selection criterion is linked to maximizing the minimum eigenvalue λ_{\min} of the history stack $Z_k = [\Phi_1, \dots, \Phi_p]$ at any k^{th} time step. In the above expressions $p \in \mathbb{N}$ denote the subscription of the last stored point. Φ_j stands for the related history stack column that is recorded at the j^{th} time step where Z_j denotes the entire history stack at the same time instant. The maximum stack span is denoted by \bar{p} which is the maximum allowable value of p and for the convergence of weights $\bar{p} \geq m$ must be satisfied where m is the rank of the uncertainty basis.

The SVM algorithm adds any sufficiently different point to the stack until the stack is full. Once the stack is full, the algorithm overwrites only if the upcoming data increases the minimum eigenvalue of the symmetric matrix Ω (and resultantly Z_k) when it is replaced with one of the existing points. In order to assure whether the upcoming data is sufficiently different from the existing data, the following norm condition is checked

$$\frac{\|\Phi(\zeta(t)) - \Phi_p\|^2}{\|\Phi(\zeta(t))\|^2} \geq \sigma \quad (4.32)$$

where σ is a case dependent constant. SVM algorithm is employed whenever this norm condition is met. The SVM algorithm is given as a flowchart below.

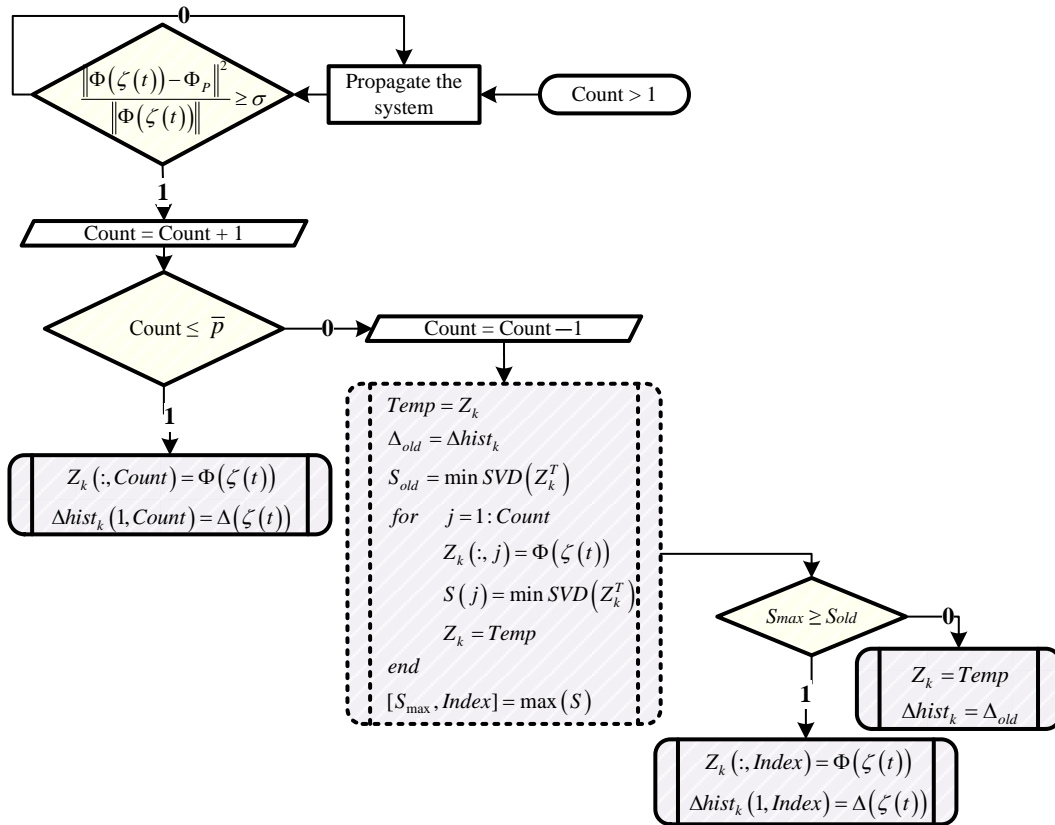


Figure 4.4-1 Singular Value Maximizing Algorithm Flow Chart

The concurrent learning algorithm is tested for structured and unstructured uncertainty with singular value maximizing data recording strategy. The same linear case that is analyzed in the previous sections is generated, roll angle and roll rate responses are given in Figure 4.4-2.

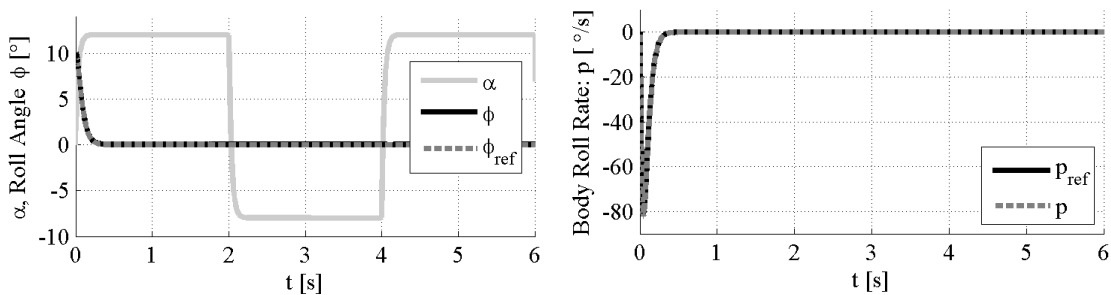


Figure 4.4-2 Linear Simulation Roll Angle, Roll Rate and Angle of Attack Responses of Concurrent Learning MRAC

Despite the drastic angle of attack profile, plant is able to track the reference model. The initial roll angle is set to 10° and the roll autopilot tries to hold the roll angle and the roll rate at 0 during the whole flight. The disturbance induced by α is shown below with the corresponding adaptive control input. Adaptive controller is able to produce the exact necessary control input within the first 2 seconds and the disturbance is cancelled uniformly.

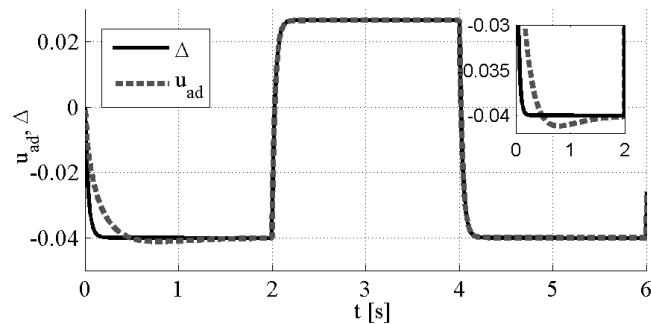


Figure 4.4-3 Structured Uncertainty and Adaptive Control Input Histories of Concurrent Learning MRAC

The main benefit of the learning algorithm manifests itself with weight history which is given in Figure 4.4-4. The weights of the Chebyshev polynomial basis function converge to their true values. Concurrent adaptive controller outperforms the classical MRAC in terms of identifying the disturbance. In classical MRAC applications there is no guarantee for weight convergence without requiring PE conditions, but concurrent learning algorithm is able to catch enough valuable information about the dynamics of the disturbance and learns eventually. The learning is completed in around 15s which is relatively high and this time could be shortened with a short maneuver in roll channel since this will provide more information to the algorithm in terms of the error between the plant model and the reference model.

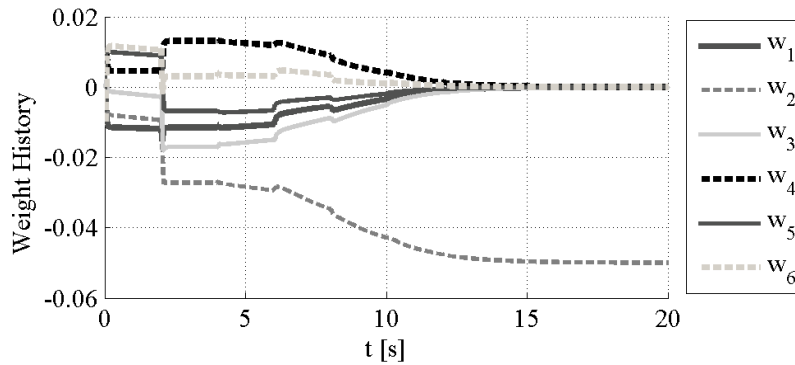


Figure 4.4-4 Adaptive Weight Histories of Concurrent Learning MRAC

As seen in Figure 4.4-5, the history stack is filled in the very beginning of the simulation and the algorithm maximizes the minimum singular value of the history stack from thereon which is shown in Figure 4.4-6. The major singular value increase is seen where the sharp angle of attack changes occurs which is due to the angle of attack dependent uncertainty parameterization.

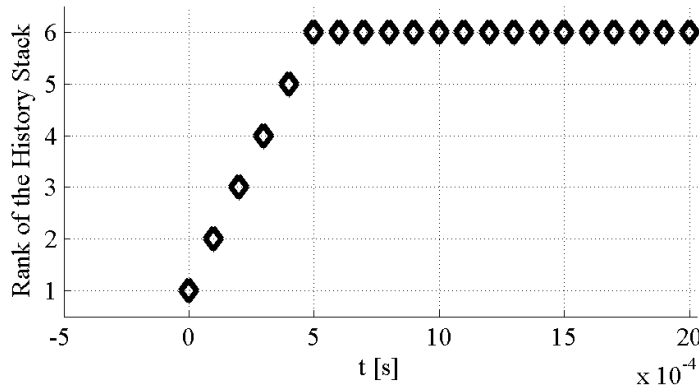


Figure 4.4-5 Rank of the History Stack

The main issue about the singular value maximizing process is the order of the minimum singular value which is highly dependent on the normalization of the Chebyshev variable mostly. The Chebyshev variable should be normalized in its

expected interval which is chosen as $\pm 15^\circ$ angle of attack in this case. If the normalization interval is chosen much wider than the expected operational envelope, the expected uncertainty domain could not be covered entirely since the upcoming information belongs to a small portion of the normalized domain. This situation causes the order of the singular value to be very low so that it becomes impossible to capture the increase with commonly used hardware in missiles.

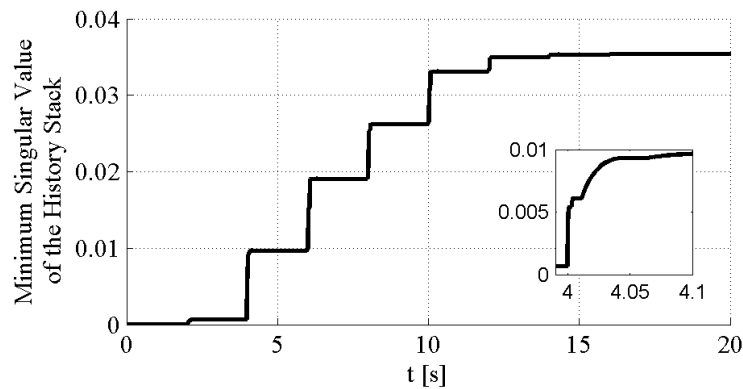


Figure 4.4-6 Minimum Singular Value of the History Stack

During this study, it is also realized that increasing stack size or decreasing step size help to increase the order of singular value. It stems from the fact that missiles and munitions have rapidly changing dynamics with short transient periods and the learning algorithm reads the changes in the system to enhance the controller performance. Hence, a transient region dominated process is more desired than a steady state region dominated process for the sake of learning. But in missiles, the information gathering part of the flight, which is the transient part mostly, does not last long. Decreasing step size could lead to an increase in singular value since it means during the same limited transient region, learning algorithm is able to iterate more and learns faster. In a similar way, increasing stack size allows storing more information; hence increases the minimum singular value of the history stack and expedites learning. However increasing stack size beyond to a limit makes decreasing step size inevitable to increase precision and also delays the contribution

of the concurrent learning since the adaptive control input is generated via online data only until the stacks are full.

It is concluded that despite the fact that MRAC and concurrent learning aided MRAC could be tuned to work well under nominal conditions for linear simulations. Concurrent learning aided MRAC distinguishes with elimination of PE condition for parameter convergence whereas the absence of PE condition leads to parameter drifts and bursting phenomena in classical MRAC scheme [53]. There are several methods in the literature to prevent bursting and parameter drift such as σ and e modifications [2]. They basically increase the damping on the weight update law which could restrict their effectiveness for particular cases. Increased damping could prevent bursting but it also makes the convergence harder and sometimes obstructs it especially if the weights do not scatter in the near neighborhood of 0 which is the usual initial condition setting for adaptive weights. The nonlinear comparison of the introduced control schemes take place in the next chapter and the discussion is elevated to a point further.

4.4.3 Effect of the Span of Basis and History Stack Size on Learning

The learning performance of the algorithm depends on few parameters besides the idea of merging the past and the current data. These parameters are size of the history stack, span of the basis function, learning rate and the eligibility condition for data recording. The structure of the basis and consequently the number of terms in the basis are strictly definite for structured uncertainties. But, for unstructured certainties the uncertainty is parameterized with a chosen basis function and if there is no clue about the complexity of the disturbance, the necessary number of terms is decided iteratively with intuition. In this study Chebyshev polynomial expansions are chosen as basis and the uncertainty is expressed with the first 6 terms of the Chebyshev polynomial expansion. The insufficient basis span could prevent learning whereas the excessive basis span could lead to overparameterization which manifests itself with oscillating weights. Hence the number of terms in a basis i.e. the span of the

basis should be carefully decided. The effects of history stack size and the basis span on learning is given in the following figure.

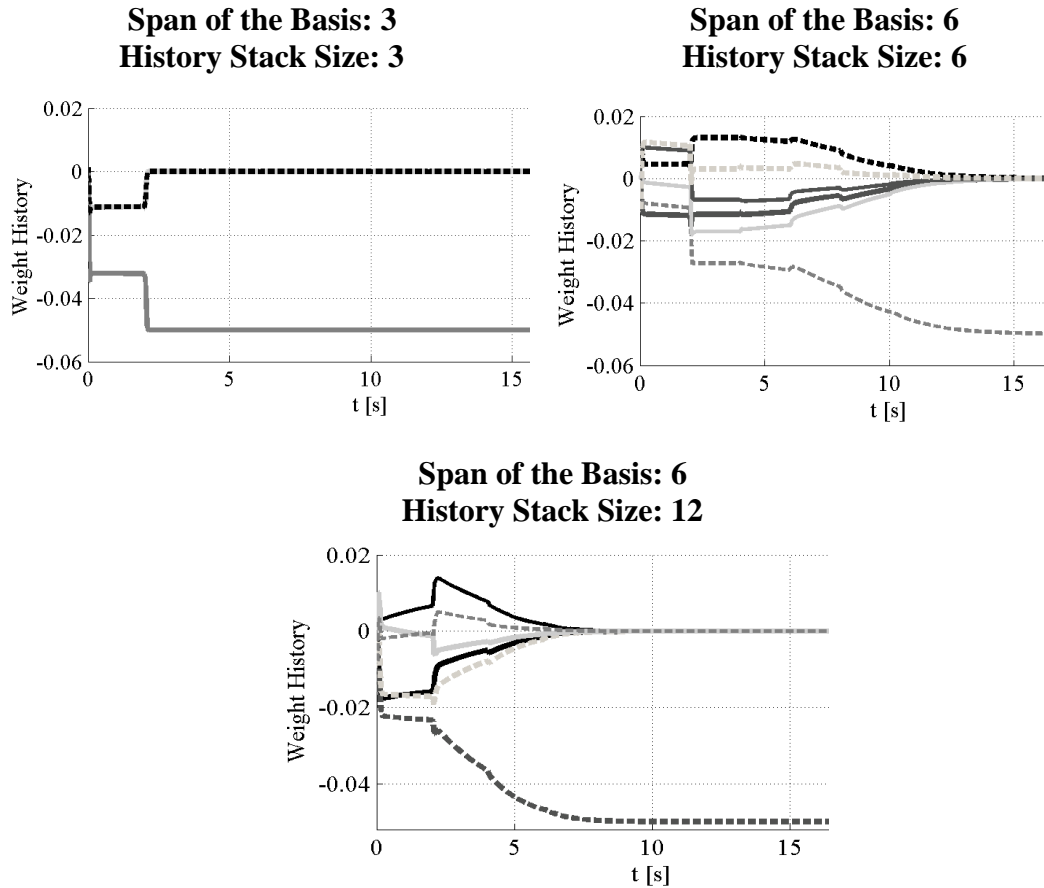


Figure 4.4-7 Effects of Basis Span and History Stack Size on Learning

The same scenario is repeated with different sizes of basis and different stack sizes in the linear simulation. The uncertainty in the linear simulation is expected to be a 1st degree polynomial, since it is added to the system using the linear relation between the rolling moment coefficient and the angle of attack. When the basis is restricted with 3 terms and an equal size of history stack is used, the algorithm learns the uncertainty at $t = 2s$. However, when the basis is generated with the first the 6 terms of the Chebyshev polynomial and an equal sized stack is employed, the algorithm learns the disturbance at $t = 15s$. This is occurred because of the unnecessarily crowded basis function. But the bottom figure shows that if the stack size is

increased to the beyond of the basis span, the weights converge at $t=8s$. By taking into consideration the above findings, it could be concluded that the number of terms in the basis should be selected wisely. Also as the stack size increases, the algorithm tends to learn faster, but the stack should be enlarged more rapidly as the basis span increases for faster convergence.

CHAPTER 5

SIMULATION RESULTS

In the previous chapters, the induced roll moment and related problems are explained in detail; the possible control solutions are discussed and applied to the current problem in linear domain. In this chapter, the controllers are tested in a more realistic nonlinear model. To assess the performance of the controllers, a 6 degree of freedom nonlinear flight simulation is built. The performance tests are generally set to make the missile do compelling maneuvers which force the linear limits of the aerodynamic database to expose the dynamic couplings. The missile is forced to undergo high angle of attack necessary maneuvers that excite pitch-roll couplings and the roll controllers are assessed in terms of their capability to hold the missile stable or to achieve the commanded roll angles. In the simulation, the sensors are assumed to be perfect and the control actuation system is a second order servomechanism which is able to execute the autopilot outputs in this study without being saturated.

5.1 Roll Control of the Guided Munition with Baseline Roll Autopilot during Compelling Longitudinal Maneuvers

5.1.1 Roll Control with Cascaded Autopilot

In this section, the pitch-roll coupling that is partially modelled in the linear domain in previous chapter is reproduced in nonlinear simulation. A large and small longitudinal acceleration command series are sent to the pitch autopilot to trigger angle of attack dependent induced roll motion. In the lateral plane, yaw channel is held stable with 0 m/s^2 acceleration command. The commanded roll angle and the

response of the roll autopilots are shown below for the cascaded roll autopilot and its feedforward augmentation.

The scenarios are composed of $\pm 1g$ (case-1) and $\pm 0.25g$ (case-2) longitudinal repetitive acceleration commands with $0 g$ lateral acceleration command while keeping the roll angle at zero except the $\pm 10^\circ \phi$ commands at $5s \leq t \leq 9s$. The munition is released from $5000 m$ with an initial velocity $0.85 M$. Flight path of the munition, Mach and θ profiles are given as follows.

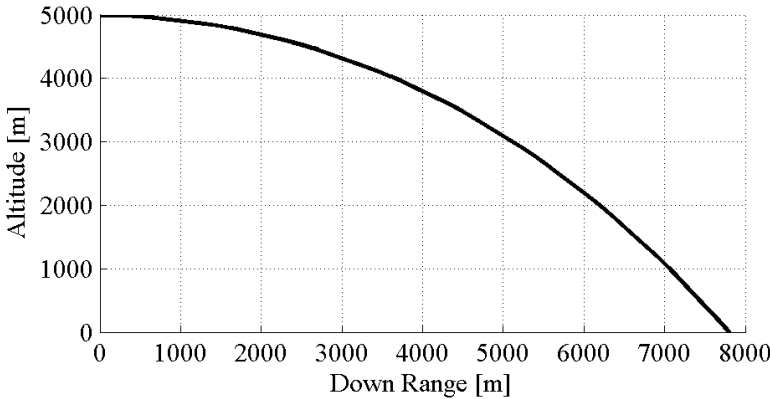


Figure 5.1-1 Flight Path of the Munition

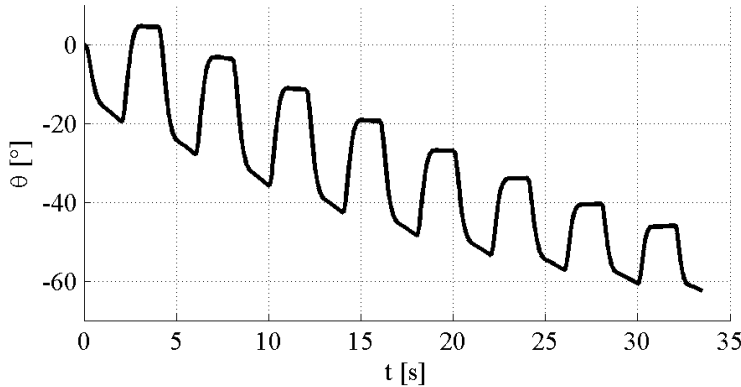


Figure 5.1-2 Elevation Angle Profile of the Munition

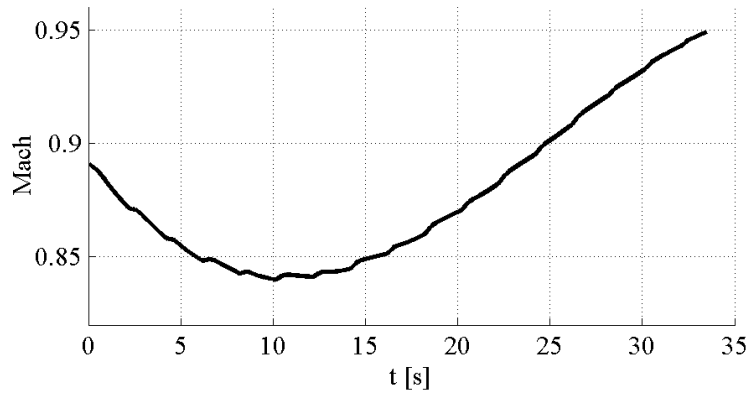


Figure 5.1-3 Mach Profile of the Munition

The control is begun as soon as the munition is separated from the host vehicle. The aerodynamic interaction between the host vehicle and the munition during the separation is assumed to be kept at minimum and is not modelled in the simulation. The longitudinal and lateral acceleration responses are shown in Figure 5.1-4 and Figure 5.1-5.

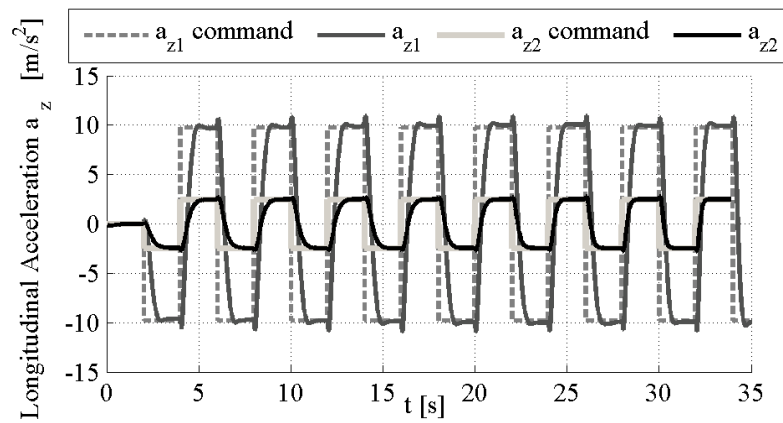


Figure 5.1-4 Cascaded A/P Longitudinal Acceleration Responses

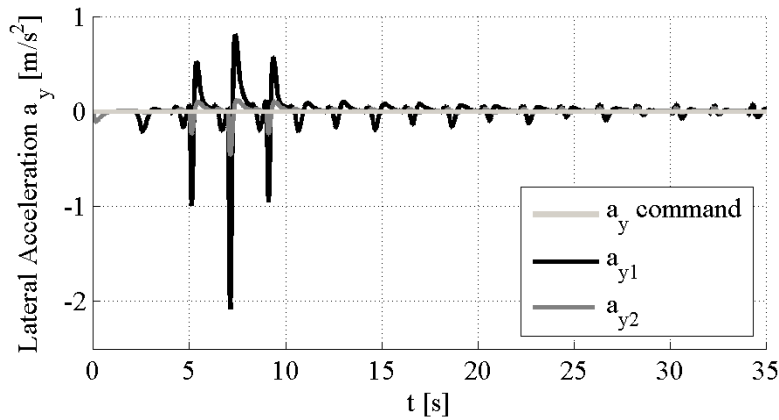


Figure 5.1-5 Cascaded A/P Lateral Acceleration Responses for Case-1 and Case-2

The longitudinal acceleration autopilot is able to track the assigned commands and the roll stabilization problem which violates the decoupled axes assumption is not apparent on the pitch autopilot responses. But, the lateral acceleration autopilot is disturbed during simultaneous commands on pitch and roll channels. The angle of attack and side slip angle histories are shown in Figure 5.1-6 and Figure 5.1-7.

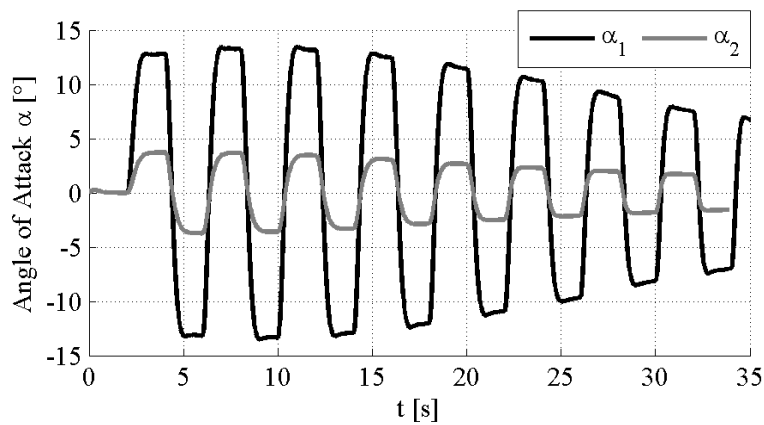


Figure 5.1-6 Cascaded A/P Angle of Attack Histories for Case-1 and Case-2

The angle of attack varies between $\pm 13^\circ$ and $\pm 4^\circ$ at most for different scenarios and amplitude is in a descending trend which is a result of increasing velocity,

descending altitude and consequently increasing aerodynamic effectiveness. The munition is able to achieve the commanded acceleration with less control surface deflection and less angle of attack through the end of the flight. The side slip angle is disturbed most during the synchronized roll-pitch commands. The pitch acceleration commands are not dominant on yaw channel which is obvious from the significantly decreasing disturbance amplitude with $0^\circ \varphi$ command after $t=9s$.

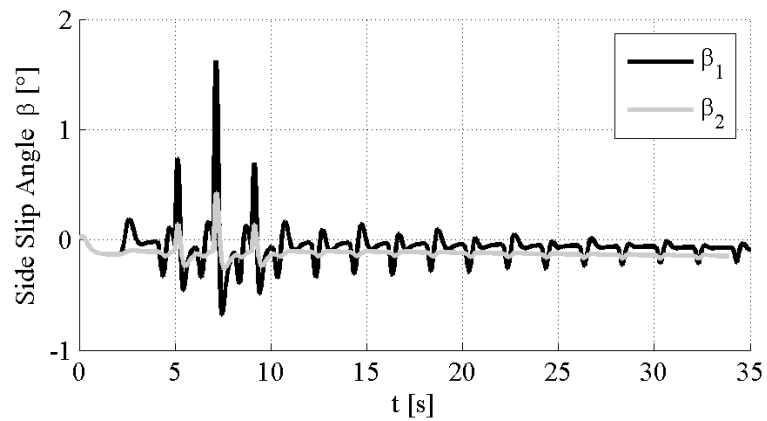


Figure 5.1-7 Cascaded A/P Side Slip Angle Histories for Case-1 and Case-2

The body roll rate and roll angle responses are shown in Figure 5.1-9 and Figure 5.1-8.

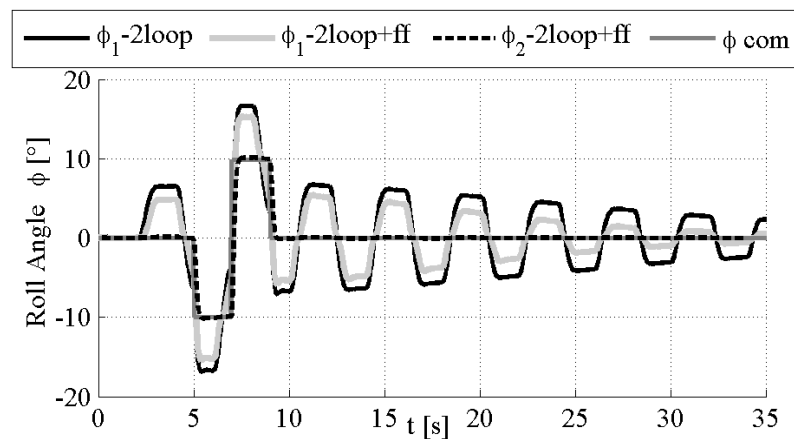


Figure 5.1-8 Cascaded A/P Roll Angle Responses for Case-1 and Case-2

The cascaded roll autopilot could not hold the roll angle at near neighborhood of 0° and likewise could not track the $\pm 10^\circ$ roll angle command with cascaded roll autopilot. The feedforward augmented cascaded roll autopilot is proven to function in linear domain but the linearity of the angle of attack and the body axis roll rate relation is violated with high angles of attack. The feedforward controller provides additional control authority which is the source of the difference between the roll angle responses in Figure 5.1-8; but in the nonlinear region, which is nearly the region where $|\alpha| \geq 5^\circ$, the amount of additional necessary control is more than the already provided amount. It is seen in both body axis roll rate and roll angle responses that, the linear α - p relation becomes valid with the decrease of the angle of attack which is through the end of the simulation for the case-1. Hence for the first case, the induced roll rate and roll angle are cancelled more effectively in the last parts.

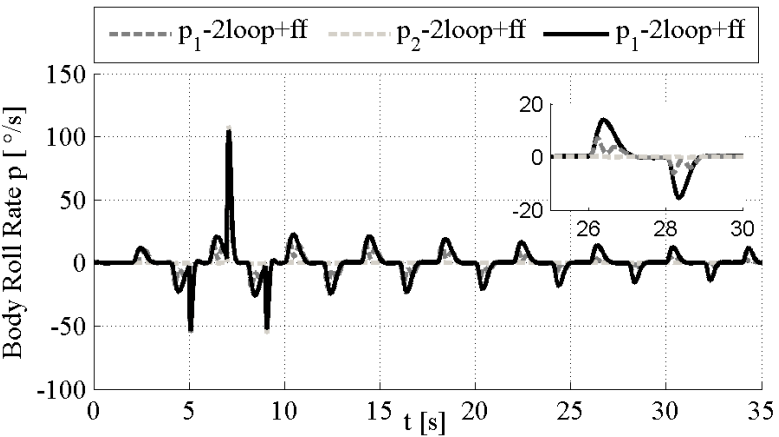


Figure 5.1-9 Cascaded A/P Roll Rate Responses for Case-1 and Case-2

The operation envelope of the guided munition involves widely varying angles of attack and side slip angles due to their limited aerodynamic effectiveness because of the absence of a thrust source. Despite the fact that the feedforward control augmented baseline scheme is effective in the near neighborhood of the linear region,

the poor performance of it during the compelling longitudinal maneuvers makes this scheme insufficient for the handled problem.

5.1.2 Roll Control with MRC

In this section, the model reference controller is used in the same scenario. The autopilot is expected to enhance the roll control performance. The pitch acceleration command is a square wave with $\pm 1g$ amplitude to excite the angle of attack induced disturbances on the system. The roll angle and the roll rate responses are given below.

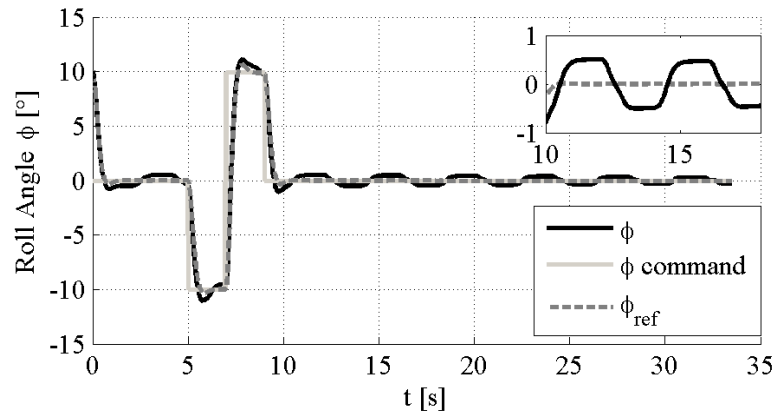


Figure 5.1-10 MRC Roll Angle Responses

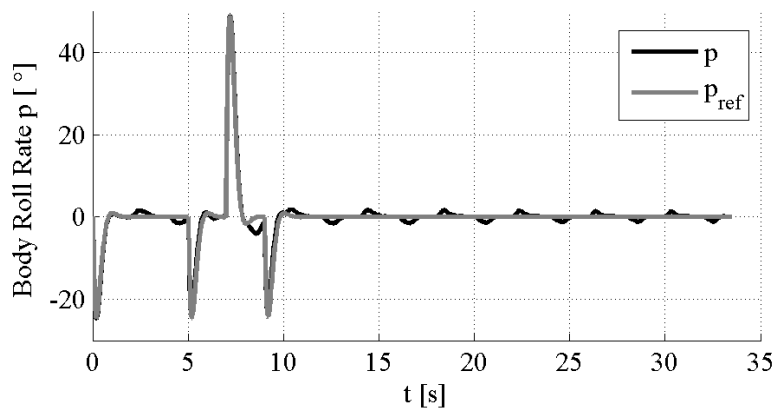


Figure 5.1-11 MRC Roll Rate Responses

The nonlinear and linear responses of MRC scheme are very similar, the disturbance induced by angle of attack is taken under control with model reference control scheme but it is seen it could not be cancelled out completely. There is a still a remaining bias on the roll angle and roll rate responses which brings forth the need for the adaptive augmentation. In the following case, the induced roll motion is tried to be controlled with a classical MRAC scheme and an MRAC based concurrent learning controller algorithm.

5.2 Adaptive Roll Control of the Guided Munition during Compelling Longitudinal Maneuvers

In this section, the scenario defined in the previous section is handled with adaptive controllers in the roll channel.

5.2.1 Roll Control with Classical MRAC

The roll angle and the roll rate histories are shown in the following figures. When the results are compared, it is realized that MRAC works better against the angle of attack induced disturbances than the MRC. Body roll angle is driven to 0 from an initial of 10° and the system is able to track the reference model. The roll rate tracking performance is also better than the MRC case, but it is apparent that the main improvement is originated from the upgraded baseline control scheme. Replacing the cascaded controller with model reference controller contributes most but could not remove the disturbance entirely where the adaptive scheme cancels out the remaining roll angle oscillations.

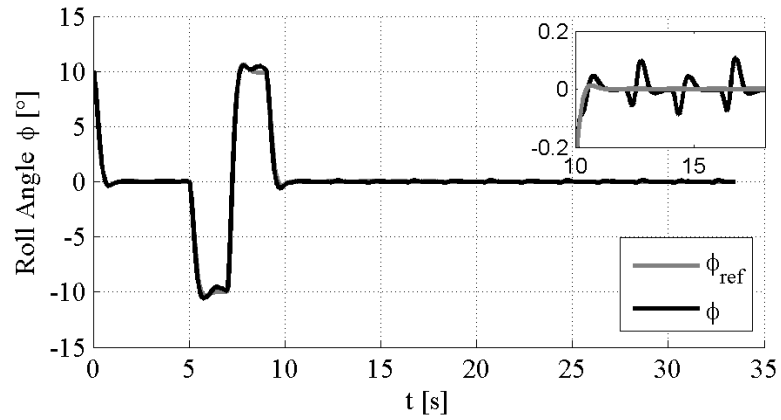


Figure 5.2-1 MRAC Roll Angle Responses

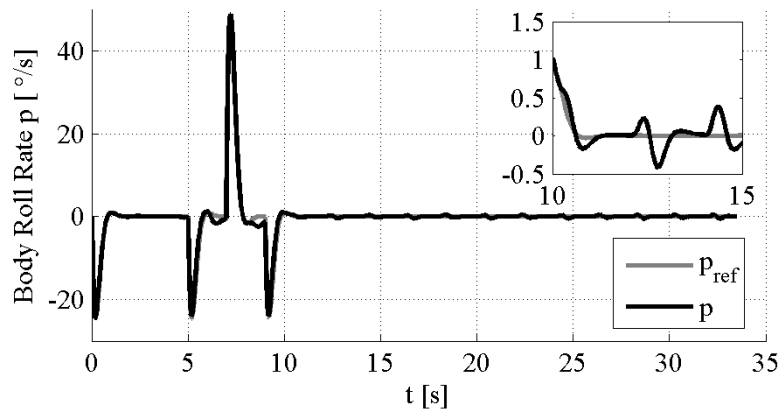


Figure 5.2-2 MRAC Roll Rate Responses

The weight history of the MRAC shows that either excited or not, the weights are not in a converging trend which proves that the current application of classical MRAC scheme is not able to learn the disturbance. It rather produces the necessary control input at every time instant without reaching the true combination of the weights.

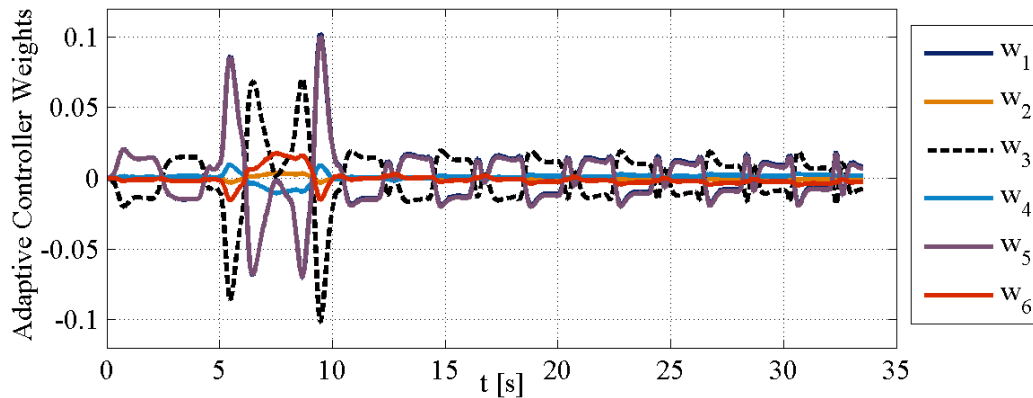


Figure 5.2-3 MRAC Adaptive Weight Histories

5.2.2 Roll Control with Concurrent Learning Aided MRAC

The roll angle and the roll rate histories are shown in the following figures.

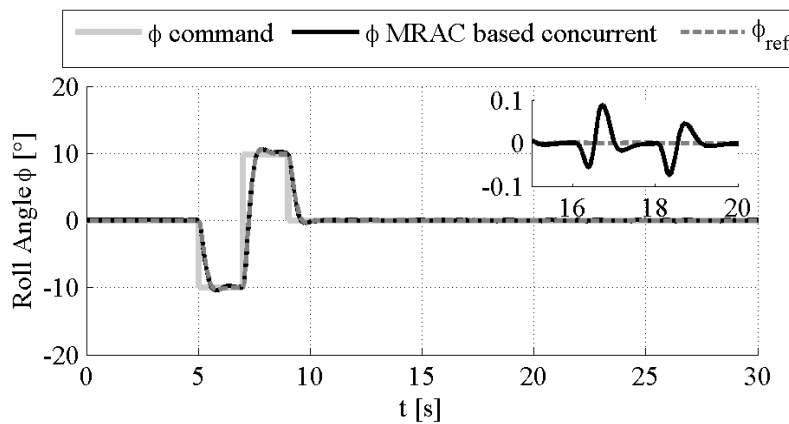


Figure 5.2-4 Concurrent Learning MRAC Roll Angle Responses

In Figure 5.2-4, the roll angle responses of the reference model and the MRAC based concurrent learning adaptive roll autopilot are shown. The reference model is chosen as a second degree transfer function with 5.5 rad/s bandwidth and 0.7 damping ratio. It is seen that the plant is able to track the roll angle response of the reference model.

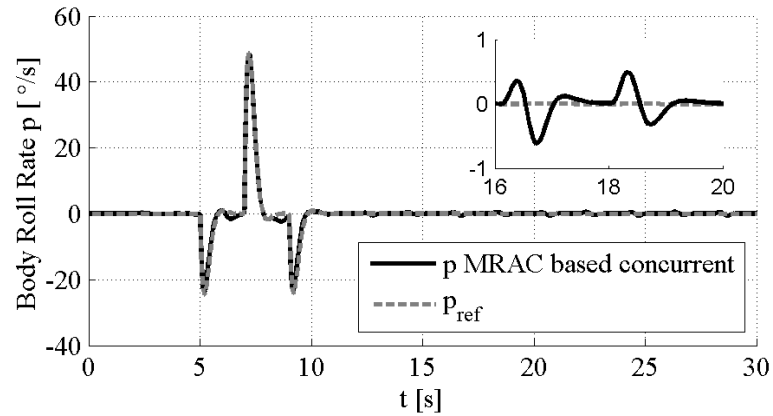


Figure 5.2-5 Concurrent Learning MRAC Roll Rate Responses

Similarly, the roll rate responses of the reference model and the plant are similar. The angle of attack is varying between -13° and 13° and the munition is subjected to 26° α variation at some parts of the simulation. This rapid change is apparent in both roll angle and roll rate responses and shown in the zoomed axes. However, it is shown that the concurrent learning adaptive autopilot is able to suppress the dramatic disturbances due to the high angle of attack profile of the simulation

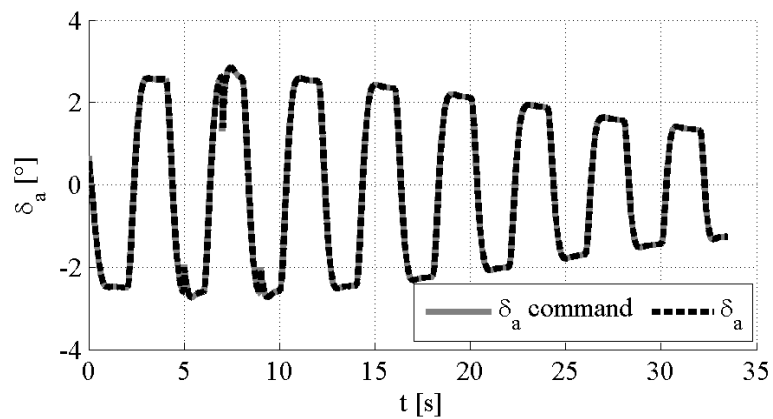


Figure 5.2-6 Aileron Command and Response

The control input command of the roll autopilot and the response of the actuator is given in Figure 5.2-6. It is seen that the actuator is able to track the autopilot commands without being saturated. The concurrent learning algorithm uses the past and current data to generate the adaptive control input. The valuable past data is stocked in the history stack by means of singular value maximizing algorithm. This algorithm ensures that the upcoming stack candidate data is useful and adequately different from the existing ones that already stocked in the memory. To check the validity of this condition, the minimum singular value of the history stack is inspected in Figure 5.2-7. The minimum singular value is in an ascending trend which proves that the algorithm works as expected. The minimum singular value is in a scale of $1e^{-12}$ which requires very sensitive hardware devices to make a decision algorithm depending on that variable in real applications.

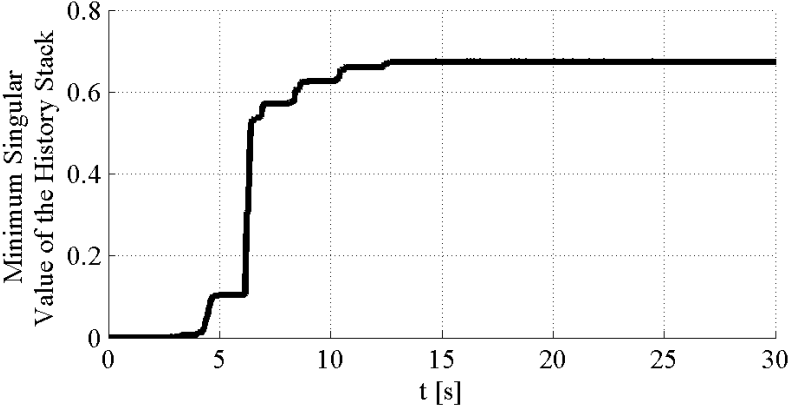


Figure 5.2-7 Concurrent Learning MRAC Minimum Singular Value of the History Stack

A history stack that is employed to record the useful past data could use many different strategies. The stack could be generated unbounded theoretically to simplify the learning algorithm by excluding the information adequacy assessment. But this application needs an infinite memory or a very high data storing capacity in real case and brings about heavy computational workload. To prevent the computational wind up, a bounded cyclic data recording algorithm could be preferred which overwrites

the upcoming data onto the existing data when the stack is full even if the upcoming information is less valuable in terms of identification of the disturbance. Nonetheless, this algorithm does not contribute enough to the learning in every control application such as our case. Depending on them, a minimum singular value maximizing history stack algorithm is applied to the studied adaptive control scheme. The stack is arranged to record 10 sufficiently different data. The sufficiently different data means that the stack is full rank once the stack is full. The rank condition is shown in Figure 5.2-8

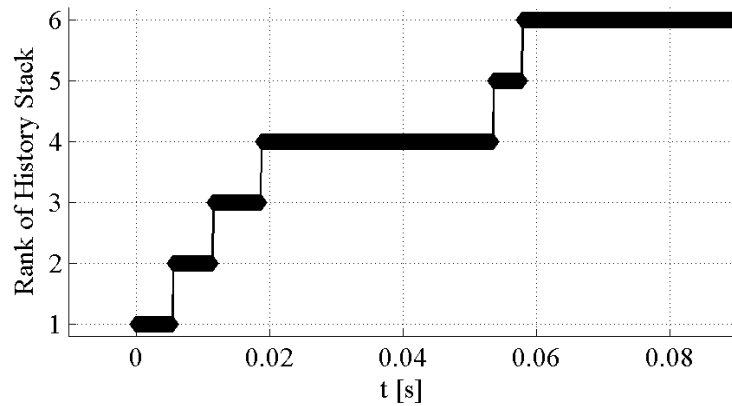


Figure 5.2-8 Concurrent Learning MRAC Rank of the History Stack

The history stack is full rank after $t=2.3s$ which is the very beginning of the simulation and the existing information is updated when a more useful data is caught. The learning ability of a parameter estimation scheme is assessed by means of convergence of the adaptive weights. The weight history is given in Figure 5.2-9. When the disturbance is introduced to the system at $t=2s$, the weights tend towards their true values and after the 9th second, the weights converge and remain stable in a small uncertainty band. Since the uncertainty is unstructured, the true values of the weights are not known but the learning performance could be interpreted with convergence.

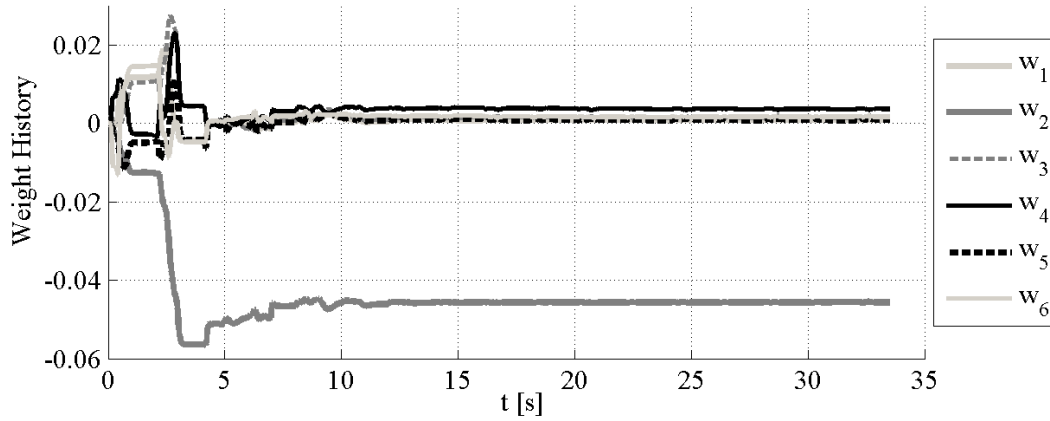


Figure 5.2-9 Concurrent Learning MRAC Adaptive Controller Weights

The alpha dependent uncertainty is obtained as follows in linear and nonlinear simulations.

Nonlinear Model Uncertainty

$$\Delta_{NL}(\bar{\alpha}) = 0.0009T_0 - 0.0457T_1 + 0.0015T_3 + 0.0036T_4 + 0.0009T_5 + 0.0016T_6 \quad (5.1)$$

Linear Model Uncertainty

$$\Delta_L(\bar{\alpha}) = -0.05T_1 \quad (5.2)$$

where;

$$\begin{aligned} T_0 &= 1 \\ T_1 &= \bar{\alpha} \\ T_2 &= 2\bar{\alpha}^2 - 1 \\ T_3 &= 2\bar{\alpha}(2\bar{\alpha}^2 - 1) - \bar{\alpha} = 4\bar{\alpha}^3 - 3\bar{\alpha} \\ T_n &= 2\bar{\alpha} \cdot T_{n-1} - T_{n-2} \\ &\vdots \end{aligned} \quad (5.3)$$

The alpha dependent uncertainty functions with respect to the angle of attack are shown below. It is obvious that when the angle of attack is small, both of the two functions give similar results, nevertheless as the angle of attack increases, the

nonlinear simulation based uncertainty function differs from the other one. This clarifies that both uncertainty functions perform well in linear region whereas the disturbance for the whole angle of attack envelope could be identified truly only in the nonlinear simulation.

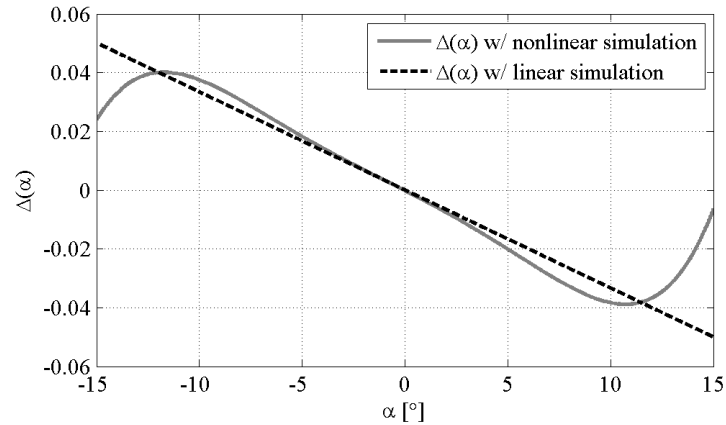


Figure 5.2-10 The Uncertainty Function Learned from Nonlinear and Linear Simulations.

5.2.3 Comparison of the State Dependent Uncertainty Parametrization with the Angle of Attack Based Uncertainty Parameterization

In this section, the effect of the uncertainty parameterization is handled. The square wave acceleration command is repeated in the longitudinal channel and the roll channel reference is kept the same. The learning rates, sampling rate, stack size and basis span are preserved whereas the uncertainty parameterization is changed. The uncertainty is assumed to be a Chebyshev polynomials based function of the states instead of angle of attack.

- Basis function generation using Chebyshev polynomial expansion for single-variable functions

$$f(x) = \sum_{i=1}^{N-1} c_{ji} T_i(x) \quad \Rightarrow \quad \begin{aligned} f(\bar{\alpha}) &= \sum_{i=1}^N w_i \Phi_i(\bar{\alpha}) \\ &= W^T \cdot \Phi(\bar{\alpha}) \end{aligned} \quad (5.4)$$

- Basis function generation using Chebyshev polynomial expansion for multi-variable functions

$$f(x, y) = \sum_{j=1}^{M-1} \sum_{i=1}^{N-1} c_{ji} T_i(x) T_j(y) \quad \Rightarrow \quad \begin{aligned} f(\bar{\phi}, \bar{p}) &= \sum_{j=1}^M \sum_{i=1}^N w_{ji} \Phi_i(\bar{\phi}) \Phi_j(\bar{p}) \\ &= W^T \cdot \text{kron}(\Phi(\bar{\phi}), \Phi(\bar{p})) \end{aligned} \quad (5.5)$$

The roll angle and the roll rate responses are given below.

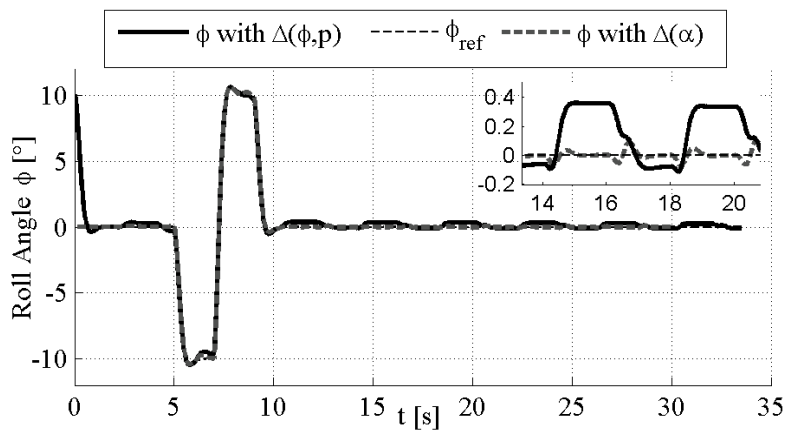


Figure 5.2-11 Roll Angle Responses with the State Dependent Uncertainty Parameterization

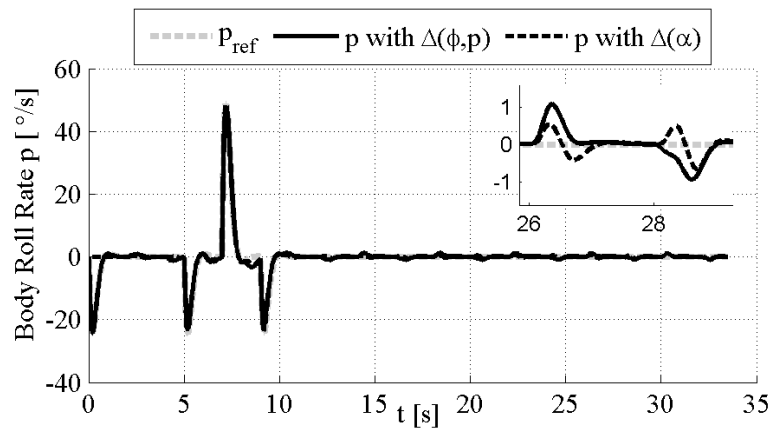


Figure 5.2-12 Roll Rate Responses with the State Dependent Uncertainty Parameterization

The roll rate, roll angle responses and the weight histories show that the uncertainty could not be removed and could not be learned completely with state dependent uncertainty parameterization if the stack size and the basis span are kept constant.

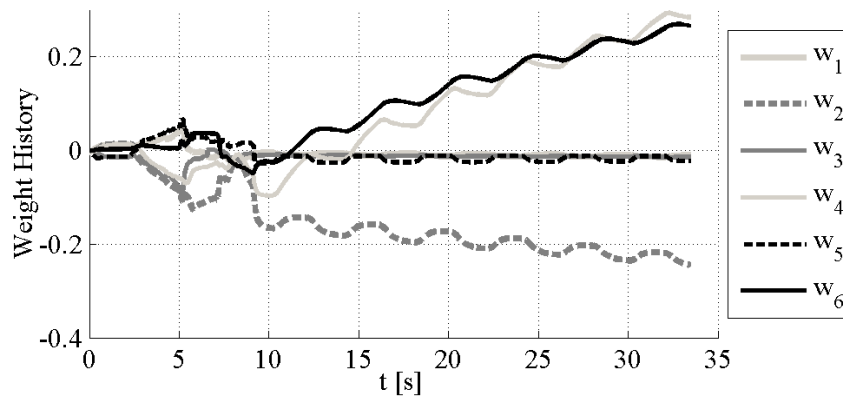


Figure 5.2-13 Weight Histories with State Dependent Uncertainty Parameterization

In order to remove the uncertainty with state dependent uncertainty parameterization, the basis should be enriched which is less effective in terms of computational effort. Also an increase in basis span usually requires higher sampling rates, which is less desired. In the light of these facts it is concluded that if the dominant source of the

uncertainty is known, the uncertainty could be expressed more effectively using a parameter that is directly related to this source as the uncertainty variable.

5.2.4 Verification of the Uncertainty Model

The difference between the uncertainty functions in linear and nonlinear simulations stems from the nonlinearity that is not apparent on the linear database. In order to prove this, the aerodynamic database of the nonlinear simulation is linearized where the angle of attack dependent uncertainty is added to the roll dynamics through the static rolling moment coefficient C_L .

$$\begin{aligned}
 C_L^{nonlinear} &= f(M, \alpha, \beta, \delta_a) \\
 C_L^{modified\ linear} &= C_{L\delta_a} \cdot (\delta_a + \Delta(\bar{\alpha})) \\
 C_L^{linear} &= C_{L\delta_a} \cdot \delta_a
 \end{aligned}
 \tag{5.6}$$

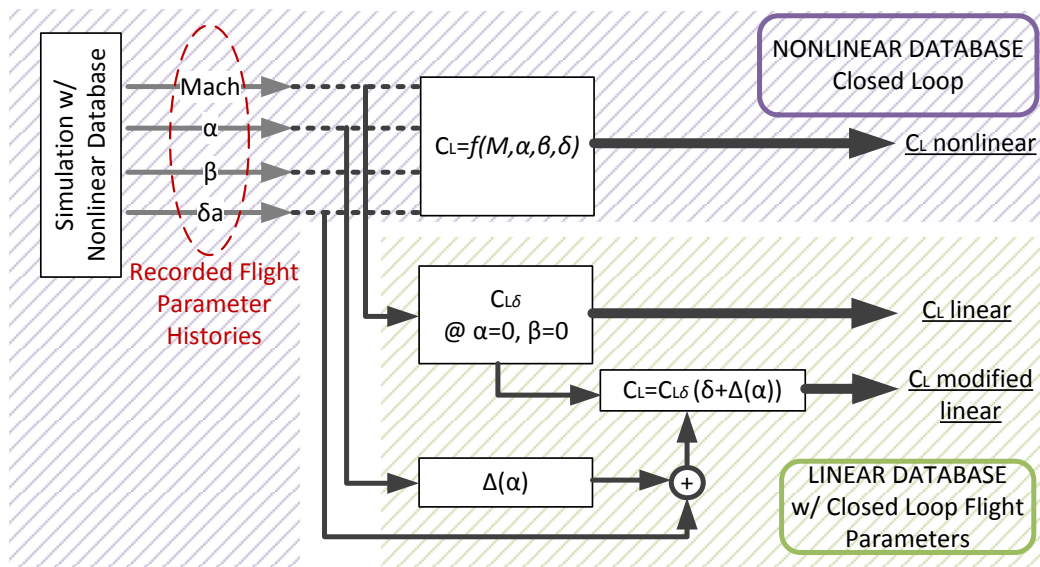


Figure 5.2-14 Verification of the Uncertainty Model

The roll damping C_{Lp} is a function of Mach number and is independent of angle of attack. The nonlinear C_L is the rolling moment coefficient belongs to the closed loop run and the flight parameters of that run are recorded and fed to the open loop aerodynamic derivative calculation. The uncertainty is estimated with the recorded angle of attack history. The flowchart of the verification process is given in the above figure.

Modified linear, linear and nonlinear rolling moment coefficients are given below.

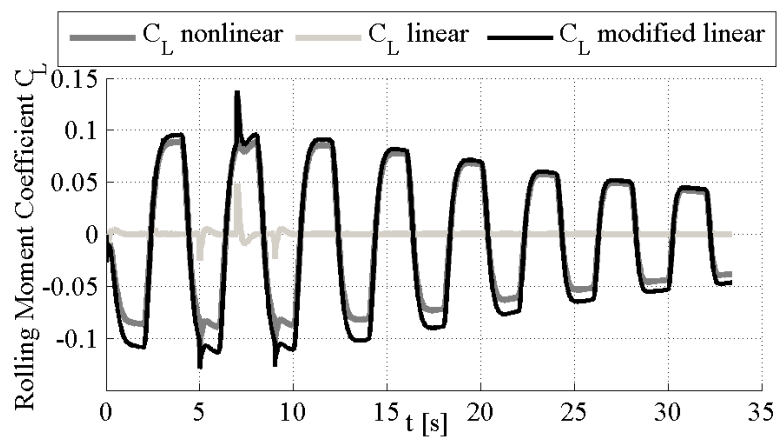


Figure 5.2-15 Rolling Moment Coefficient Histories with Linear, Nonlinear and Modified Linear Databases

The linear C_L shows a similar behavior to the angle of attack history because of the produced aileron commands against the uncertainty in the closed loop. But since the uncertainty is not included in the linear C_L , it does not give similar results to the nonlinear C_L . However, the modified linear C_L is very similar to the nonlinear C_L . The small difference between them stems from the linear assumptions but the modified linear and the nonlinear coefficients are close enough to comment that the uncertainty function is a sufficiently good model of the actual uncertainty.

It is not meaningful to compare closed loop responses since the controller is adaptive against the alpha dependent uncertainty and diminishes it even the uncertainty model

is different than the original uncertainty but it is presented to give the reader an idea about the similarities in the transient parts.

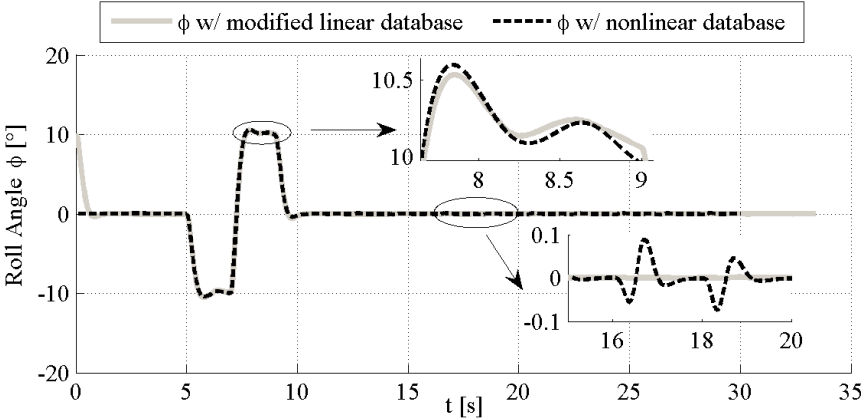


Figure 5.2-16 Roll Angle Responses with Modified Linear and Nonlinear Databases

It is realized that the results are rather similar with the modified linear and the nonlinear databases except that the peaks at the zero command parts of the nonlinear database aided simulation are not obvious in the modified linear database aided simulation. Those peaks occur simultaneously with the pitch acceleration commands but since the obtained nonlinearity level is limited, the peaks are not apparent on the modified linear database aided responses.

CHAPTER 6

CONCLUSION AND FUTURE WORK

In this thesis, adaptive control solutions for the roll channel control of guided munitions have been presented. Guided munitions are enhanced versions of traditional iron bombs with GPS, INS and seeker integrations. The additional components enhance the target hit capability of the munition significantly but they bring along some aerodynamic challenges as well. The cross-coupled interactions are triggered with the sharp maneuvers and the stabilization of the roll channel is aggravated consequently. The decoupled aerodynamics assumption which is put forward for linear controller design holds no more and a significant amount of roll angle is induced with the presence of angle of attack on the munition. This study briefly focuses on the stabilization of roll channel under dominant roll-pitch couplings by means of augmentations on the roll autopilot.

In the beginning of the study, it was proved that using cascaded autopilot structure is an ineffective control strategy to overcome dominant pitch-roll couplings. The next approach was to add an aerodynamic derivative term which defines the roll moment contribution of the angle of attack and to augment the cascaded roll autopilot with a feedforward controller. The problem with this scheme was stated with the fact that the feedforward control scheme is only applicable in a small region where the linear relation between the roll rate and the angle of attack is valid. Then a the fixed-gain model reference controller scheme was applied but the perfect plant assumption of the fixed gain MRC applications made the controller impotent against the parametric uncertainties on the plant which is inevitable in real applications. Hence, to improve the robustness of MRC, adaptive augmentations were proposed. Stated by the theory, the interest of MRAC is the asymptotic command tracking and it is achieved despite

the system uncertainties. The controllers may yield transient oscillations due to higher adaption rates and weights may not resemble to the actual values. A necessary condition for the weight convergence is the persistency of excitation which brings about hard to achieve restrictions on reference input. Besides the weight convergency, a non-PE reference input may lead to instabilities such as bursting phenomenon and parameter drift. The modifications that prevent instabilities driven by non-PE condition guarantee boundedness of the adaptive weights but they also bring along redundant stiffness on the weight update law. The MRAC scheme enhances the performance of the fixed gain MRC in terms of eliminating the angle of attack dependent disturbance; but in order to relax the PE condition, concurrent learning MRAC scheme was introduced. Concurrent learning algorithm uses the past and present data together to adapt the control law weights. If the recorded data is rich enough in terms of expressing the disturbance, the weights converge to their true values without the necessity of PE condition. Concurrent learning MRAC showed similar performance to the MRAC in terms of cancelling the disturbance and also learns the uncertainty with Chebyshev polynomials basis function. In this thesis, it was shown that using Chebyshev polynomial expansion is a good strategy to identify the uncertainty which is claimed to be the best approximation method in literature because of its orthogonality property.

The main contribution of this research is the state independent uncertainty parameterization. It was shown that uncertainty parameterization independent of the system states could be a better approach depending on the case. In the studied case, angle of attack dependent uncertainty parameterization provides faster learning with a basis with less terms. Despite the fact that any uncertainty that is apparent on the states as disturbance could be modelled through the system states; it should also be possible to include the uncertainty through its directly related variable if there is one. Even though the structure of the uncertainty is unknown, usually the phenomenon inducing the uncertainty is conspicuous but it might not be expressed well with system states as happened so in this study. The idea offered in this study was to relax the assumption of the state dependent uncertainty. Defining the uncertainty with its'

conducive parameter contributed especially in identifying the unstructured uncertainties.

Concurrent learning MRAC scheme also gave an intuition that it could show superiorities over the commonly used system identification techniques for missiles. The system ID studies are generally focused on the uncertainties on the linear aerodynamic derivatives. However with concurrent learning MRAC, it could be possible to identify the nonlinear uncertainties which is more desired. The verification of the learned uncertainty shows that the nonlinearity is mainly embedded in the aerodynamic database whereas the contribution of the kinematic couplings to the nonlinearity is fewer. The detailed studies on concurrent learning aided system identification techniques are left as a follow through.

To sum up, in the first chapter, the problem is defined and the related studies that take place in the literature are summarized. In the second chapter the munition dynamics and kinematics are studied for the integrity of the content. Next, the baseline control schemes are discussed with their advantages and insufficiencies which constitute a basis for the adaptive control chapter. In the fourth chapter, the adaptive augmentations are handled in detail. Classic MRAC law and its elevation with a concurrent learning algorithm are explained and their linear domain applications are compared. In the last chapter, the aforementioned control solutions are integrated to the nonlinear simulation. To assess the performance of the controllers, a 6 degree of freedom nonlinear flight simulation is built. The performance tests are generally set to make the missile do compelling maneuvers which force the linear limits of the aerodynamic database to expose the dynamic couplings. The missile is forced to undergo high angle of attack necessary maneuvers that excite pitch-roll couplings and the roll controllers are assessed in terms of their capability to hold the missile stable or to achieve the commanded roll angles. In the end, the MRAC based concurrent learning adaptive autopilot shown important superiorities over the standard MRAC algorithm. The disturbance is expressed by using angle of attack as state and Chebyshev polynomials are used as basis function.

The roll stabilization is ensured and the weights converge to their true values which show that the disturbance is learned in a small uncertainty band. The coupling originated disturbance is learned via the Concurrent Learning MRAC scheme and this nonlinearity is added to the linear database which gives similar results to the nonlinear database. For the future studies, it is recommended to investigate the pitch-roll couplings during compelling yaw maneuvers. It is known that the yaw motion contributes to the roll coupling which is not covered considering the scope of this thesis; the related research is rather left as a follow-through.

REFERENCES

- [1] K. Narendra, Y.-H. Lin, and L. Valavani, “Stable adaptive controller design, part II: Proof of stability,” *IEEE Trans. Automat. Contr.*, vol. 25, no. 3, pp. 440–448, 1980.
- [2] E. Lavretsky and K. A. Wise, *Robust and Adaptive Control with Aerospace Applications*. 2005.
- [3] G. Chowdhary, J. How, and H. Kingravi, “Model Reference Adaptive Control using Nonparametric Adaptive Elements,” no. August, 2012.
- [4] J. Monaco, D. Ward, and A. Bateman, “A retrofit architecture for model-based adaptive flight control,” *Proc. AIAA 1st Intell. ...*, no. September, pp. 1–18, 2004.
- [5] P. Jain, “Design of a Model Reference Adaptive Controller Using Modified MIT Rule for a Second Order System,” vol. 3, no. 4, pp. 477–484, 2013.
- [6] S. Fekri, M. Athans, and A. Pascoal, “Robust multiple model adaptive control (RMMAC): A case study,” *Int. J. Adapt. Control Signal Process.*, no. 21, pp. 1–30, 2007.
- [7] E. N. Johnson and S. K. Kannan, “Adaptive Trajectory Control for Autonomous Helicopters,” *J. Guid. Control. Dyn.*, vol. 28, no. 3, pp. 524–538, 2005.
- [8] M. Steinberg, “Historical Overview of Research in Reconfigurable Flight Control,” in *Proceedings of the Institution of Mechanical Engineers, Part G: Journal of Aerospace Engineering*, 2005, vol. 219, no. 4, pp. 263–275.
- [9] H. D. Patino, R. Carelli, and B. R. Kuchen, “Neural networks for advanced control of robot manipulators,” *IEEE Trans. Neural Netw.*, vol. 13, no. 2, pp. 343–354, 2002.

- [10] K. S. Narendra and A. M. Annaswamy, "A New Adaptive Law for Robust Adaptation without Persistent Excitation," *1986 Am. Control Conf.*, vol. c, pp. 134–145, 1986.
- [11] A. J. Calise and M. Sharma, "Neural network augmentation of existing linear controllers," *AIAA Guid. Navig. Control Conf.*, no. August, 2001.
- [12] M. B. McFarland and A. J. Calise, "Neural Networks and Adaptive Nonlinear Control of Agile Antiair Missiles," *J. Guid. Control. Dyn.*, vol. 23, no. 3, pp. 547–553, 2000.
- [13] N. Kim, "Adaptive Output Feedback Control of Uncertain Nonlinear Systems Using Single-Hidden-Layer Neural Networks," *Control*, vol. 13, no. 6, pp. 1420–1431, 2002.
- [14] B. S. Kim and A. J. Calise, "Nonlinear flight control using neural networks," *J. Guid. Control. Dyn.*, vol. 20, no. 1, pp. 26–33, 1997.
- [15] M. Sharma, "A Neuro-Adaptive Autopilot Design for Guided Munitions," no. April, 2001.
- [16] P. a. Ioannou, J. Sun, and P. List, "Robust Adaptive Control," *N/a*, vol. N/A, p. 821, 1996.
- [17] G. Chowdhary and E. Johnson, "Concurrent learning for convergence in adaptive control without persistency of excitation," *Proc. IEEE Conf. Decis. Control*, no. December, pp. 3674–3679, 2010.
- [18] M. A. Duarte and K. S. Narendra, "Combined Direct and Indirect Approach to Adaptive Control," *IEEE Trans. Automat. Contr.*, vol. 34, no. 10, pp. 1071–1075, 1989.
- [19] J.-J. E. Slotine and W. Li, "Composite adaptive control of robot manipulators," *Automatica*, vol. 25, no. 4, pp. 509–519, 1989.

- [20] M. Mühlegg, G. Chowdhary, and E. Johnson, “Concurrent Learning Adaptive Control of Linear Systems with Noisy Measurements,” *AIAA Guid. Navig. Control Conf.*, no. 1, pp. 1–13, 2012.
- [21] G. V. Chowdhary and E. N. Johnson, “Theory and Flight-Test Validation of a Concurrent-Learning Adaptive Controller,” *J. Guid. Control. Dyn.*, vol. 34, no. 2, pp. 592–607, 2011.
- [22] G. Chowdhary, T. Wu, M. Cutler, N. K. Ure, and J. How, “Experimental Results of Concurrent Learning Adaptive Controllers,” *AIAA Guid. Navig. Control Conf.*, no. August, pp. 1–14, 2012.
- [23] N. Nguyen and M. Field, “Adaptive Control for Linear Uncertain Systems with Unmodeled Dynamics Revisited via Optimal Control Modification,” 2013.
- [24] N. T. Nguyen, J. Burken, and A. Ishihara, “Least-Squares Adaptive Control Using Chebyshev Orthogonal Polynomials,” pp. 1–21, 2011.
- [25] N. T. Nguyen, “Least-Squares Model-Reference Adaptive Control with Chebyshev Orthogonal Polynomial Approximation,” *J. Aerosp. Inf. Syst.*, vol. 10, no. 6, pp. 268–286, 2013.
- [26] N. T. Nguyen, K. Krishnakumar, and J. Boskovic, “An Optimal Control Modification to Model-Reference Adaptive Control for Fast Adaptation,” *Guid. Navig. Control Conf.*, no. August, 2008.
- [27] L. V Krishnamoorthy, D. R. Kirk, R. Glass, D. Science, and T. O. Australia, “An Aerodynamic Database for the Mk 82 General Purpose Low Drag Bomb,” *Aeronaut. Marit. Res. Lab. DSTO-TR-0554, Salisbury, South Aust.*, 1997.
- [28] G. Chowdhary and E. Johnson, “A singular value maximizing data recording algorithm for concurrent learning,” *Proc. 2011 Am. Control Conf.*, pp. 3547–3552, 2011.

- [29] J. S. Shamma, "Robust stability with time-varying structured uncertainty," *IEEE Trans. Automat. Contr.*, vol. 39, pp. 714–724, 1994.
- [30] J. C. D. J. C. Doyle, "Structured uncertainty in control system design," *1985 24th IEEE Conf. Decis. Control*, vol. 24, pp. 260–265, 1985.
- [31] S. Boyd and S. S. Sastry, "Necessary and sufficient conditions for parameter convergence in adaptive control," *Automatica*, vol. 22, no. 6, pp. 629–639, 1986.
- [32] C. Cao, N. Hovakimyan, and E. Lavretsky, "Application of L 1 Adaptive Controller to Wing Rock *," no. August, pp. 1–12, 2006.
- [33] J. M. Elzebda, A. H. Nayfeh, and D. T. Mookj, "Development of an Analytical Model of Wing Rock for Slender Delta Wings," vol. 26, no. 8, pp. 737–743, 1989.
- [34] C. Lin and C. Hsu, "Control of Wing-Rock Motion," vol. 25, no. 6, pp. 1163–1165.
- [35] S. N. Singh, W. Yim, and W. R. Wells, "Direct Adaptive and Neural Control of Wing-Rock Motion of Slender Delta Wings," vol. 18, no. 1, 1995.
- [36] C. Hsu and C. E. Lan, "Theory of Wing Rock," *Aircraft*, vol. 22, no. 10, pp. 920–924, 1985.
- [37] S. Joshi, A. Strenatha, and J. Chandrasekhar, "Suppression of wing rock of slender delta wings using a single neuron controller," vol. 6, no. 5, pp. 671–677, 1998.
- [38] a. H. Nayfeh, J. M. Elzebda, and D. T. Mook, "Analytical study of the subsonic wing-rock phenomenon for slender delta wings," *J. Aircr.*, vol. 26, no. 9, pp. 805–809, 1989.

- [39] G. Chowdhary and E. Johnson, “Concurrent learning for convergence in adaptive control without persistency of excitation,” in *49th IEEE Conference on Decision and Control (CDC)*, 2010, no. December, pp. 3674–3679.
- [40] C. S. Lin and C. K. Li, “A sum-of-product neural network (SOPNN),” *Neurocomputing*, vol. 30, no. September 1998, pp. 273–291, 2000.
- [41] A. T. Kutay, “Neural network based adaptive output feedback control: applications and improvements,” *Cornell Hotel Restaur. Adm. Q.*, vol. 22, no. 2, 2005.
- [42] M. Sharma and A. J. Calise, “Neural-Network Augmentation of Existing Linear Controllers,” *J. Guid. Control. Dyn.*, vol. 28, no. 1, pp. 12–19, 2005.
- [43] A. J. Calise, B. J. Yang, and J. I. Craig, “Augmentation of an existing linear controller with an adaptive element,” *Proc. Am. Control Conf.*, vol. 2, pp. 1549–1554, 2002.
- [44] S.-K. Oh, W. Pedrycz, and B.-J. Park, “Polynomial neural networks architecture: analysis and design,” *Comput. Electr. Eng.*, vol. 29, no. 6, pp. 703–725, 2003.
- [45] J. C. Mason and D. C. Handscomb, *Chebyshev Polynomials*. 2003.
- [46] B. a Pearlmutter, “Dynamic Recurrent Neural Networks,” vol. 196, no. 7330, pp. 1–32, 1990.
- [47] B. A. Pearlmutter, “Learning State Space Trajectories in Recurrent Neural Networks,” *Neural Comput.*, vol. 1, no. 2, pp. 263–269, 2011.
- [48] J. J. Steil, “Backpropagation-Decorrelation : online recurrent learning with $O(N)$ complexity,” *IEEE Int. Jt. Conf. Neural Networks*, vol. 2, pp. 843–848, 2004.
- [49] T. Mikolov, A. Joulin, S. Chopra, and M. Mathieu, “Learning Longer Memory in Recurrent Neural Networks,” *Iclr*, pp. 1–9, 2015.

- [50] J. Bayer and C. Osendorfer, “Learning Stochastic Recurrent Networks,” *Iclr 2015*, pp. 1–8, 2015.
- [51] J. Martens and I. Sutskever, “Learning recurrent neural networks with Hessian-free optimization,” *Proc. 28th Int. Conf. Mach. Learn. ICML 2011*, pp. 1033–1040, 2011.
- [52] R. J. Williams and D. Zipser, “A Learning Algorithm for Continually Running Fully Recurrent Neural Networks,” *Neural Comput.*, vol. 1, no. 2, pp. 270–280, 1989.
- [53] M. Hovd and R. R. Bitmead, “Directional leakage and parameter drift,” *Int. J. Adapt. Control Signal Process.*, vol. 20, no. 1, pp. 27–39, 2006.

APPENDIX A

BASELINE AUTOPILOT DESIGN

In this section, linearized dynamics of the missile are analyzed and the baseline autopilots are built based on the constructed linear models for the integrity of the content.

A.1 Linear Model Construction

Linear models provide decoupled sets of equations which simplify the autopilot design process and make it possible to spare the control of orthogonal motions. The equations of motion are linearized around $\alpha = \beta = 0^\circ$, $p = q = r = 0^\circ/s$ and $\delta_e = \delta_r = \delta_a = 0^\circ$ trim condition. The roll dynamics are assumed to be much faster than pitch and yaw dynamics for linearization and the longitudinal body velocity u is not assumed to be constant, in contrast to the general application. The gravitational forces are neglected considering that they are small compared to the aerodynamic forces. Small angle assumptions are made whenever applicable. Based on these assumptions, linear equations of motion are simplified as following

- Pitch Dynamics

$$\begin{bmatrix} \dot{\alpha} \\ \dot{q} \\ \dot{\delta} \\ \ddot{\delta} \end{bmatrix} = \begin{bmatrix} \frac{Z_\alpha}{mV} - \frac{\dot{u}}{u} & 1 + \frac{Z_q}{mV} & \frac{Z_\delta}{mV} & 0 \\ \frac{M_\alpha}{I_z} & \frac{M_q}{I_z} & \frac{M_\delta}{I_z} & 0 \\ 0 & 0 & 0 & 1 \\ 0 & 0 & -\omega_n^2 & -2\zeta\omega_n \end{bmatrix} \begin{bmatrix} \alpha \\ q \\ \delta \\ \dot{\delta} \end{bmatrix} + \begin{bmatrix} 0 \\ 0 \\ 0 \\ \omega_n^2 \end{bmatrix} \delta_{e_{com}} \quad (\text{A.1})$$

$$a_z = \begin{bmatrix} \frac{Z_\alpha}{m} + \frac{\dot{u}}{u} & \frac{Z_q}{m} & \frac{Z_\delta}{m} & 0 \end{bmatrix} \begin{bmatrix} \alpha & q & \delta & \dot{\delta} \end{bmatrix}^T \quad (\text{A.2})$$

- Yaw Dynamics

$$\begin{bmatrix} \dot{\beta} \\ \dot{r} \\ \dot{\delta} \\ \ddot{\delta} \end{bmatrix} = \begin{bmatrix} \frac{Y_\beta}{mV} - \frac{\dot{u}}{u} & \frac{Y_r}{mV} - 1 & \frac{Y_\delta}{mV} & 0 \\ \frac{N_\alpha}{I_y} & \frac{N_q}{I_y} & \frac{N_\delta}{I_y} & 0 \\ 0 & 0 & 0 & 1 \\ 0 & 0 & -\omega_n^2 & -2\zeta\omega_n \end{bmatrix} \begin{bmatrix} \beta \\ r \\ \delta \\ \dot{\delta} \end{bmatrix} + \begin{bmatrix} 0 \\ 0 \\ 0 \\ \omega_n^2 \end{bmatrix} \delta_{r_{com}} \quad (\text{A.3})$$

$$a_y = \begin{bmatrix} \frac{Y_\beta}{m} + \frac{\dot{u}}{u} & \frac{Y_r}{m} & \frac{Y_\delta}{m} & 0 \end{bmatrix} \begin{bmatrix} \beta & r & \delta & \dot{\delta} \end{bmatrix}^T \quad (\text{A.4})$$

- Roll Dynamics

$$\begin{bmatrix} \dot{\phi} \\ \dot{p} \\ \dot{\delta} \\ \ddot{\delta} \end{bmatrix} = \begin{bmatrix} 0 & 1 & 0 & 0 \\ 0 & \frac{L_p}{I_x} & \frac{L_\delta}{I_x} & 0 \\ 0 & 0 & 0 & 1 \\ 0 & 0 & -\omega_n^2 & -2\zeta\omega_n \end{bmatrix} \begin{bmatrix} \phi \\ p \\ \delta \\ \dot{\delta} \end{bmatrix} + \begin{bmatrix} 0 \\ 0 \\ 0 \\ \omega_n^2 \end{bmatrix} \delta_{a_{com}} \quad (\text{A.5})$$

$$\dot{\phi} = [1 \ 0 \ 0 \ 0] \begin{bmatrix} \phi & p & \delta & \dot{\delta} \end{bmatrix}^T \quad (\text{A.6})$$

In equations (A.1)-(A.6) the dimensional aerodynamic derivatives are defined as given below for longitudinal, lateral and directional dynamics.

- Longitudinal Plane Aerodynamic Derivatives

$$\begin{aligned} Z_\alpha &= QSC_{Z_\alpha} & Z_q &= QS \frac{d}{2V} C_{Z_q} & Z_\delta &= QSC_{Z_\delta} \\ M_\alpha &= QSdC_{M_\alpha} & M_q &= QSd \frac{d}{2V} C_{M_q} & M_\delta &= QSdC_{M_\delta} \end{aligned}$$

- Lateral Plane Aerodynamic Derivatives

$$\begin{aligned} Y_\beta &= QSC_{Y_\beta} & Y_r &= QS \frac{d}{2V} C_{Y_r} & Y_\delta &= QSC_{Y_\delta} \\ N_\beta &= QSdC_{N_\beta} & N_r &= QSd \frac{d}{2V} C_{N_r} & N_\delta &= QSdC_{N_\delta} \end{aligned}$$

- Directional Plane Aerodynamic Derivatives

$$L_p = QSC_{L_p} \quad L_\delta = QS \frac{d}{2V} C_{L_\delta}$$

A.2 Autopilot Design

There are many linear and nonlinear control applications for guided munitions and many of them are studied throughout the constitution of this thesis. In literature survey, outstanding studies are also mentioned. Advanced techniques are occupied whenever necessary but it is always wisely to try to solve the problem with the simplest, first. Hence, the control of guided munition is aimed to be handled via linear gain-scheduled autopilots. Since the linear autopilot is failed to overcome dynamic couplings, gain scheduling is disabled and current structure serves as a baseline controller for an adaptive adaptation.

The baseline control of the missile is handled via the control of acceleration in pitch and yaw axes. Roll autopilot serves as a regulator to stabilize the missile at $0^\circ \phi$ condition.

A.2.1 Acceleration Autopilot Design for Longitudinal and Lateral Planes

The acceleration autopilot is a full state feedback controller and aims to locate the closed loop poles of the system in order to obtain the desired transient performance. The controller is designed considering the linear aerodynamic database and control actuation system limits. The control scheme of the acceleration autopilot is given in Figure A.2-1

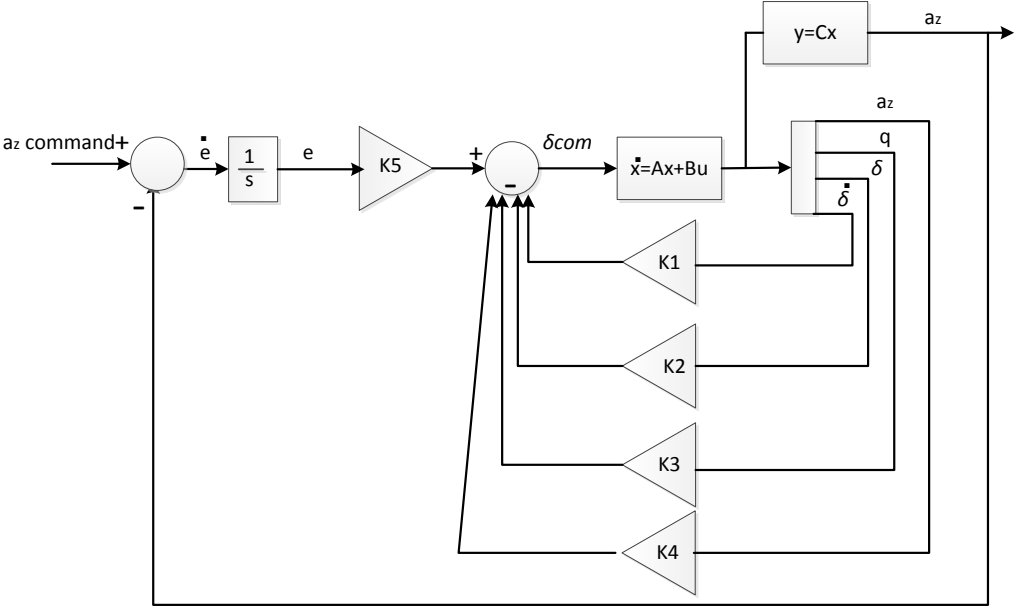


Figure A.2-1 Control scheme for longitudinal acceleration autopilot

The yaw axes acceleration autopilot is in the same form with the pitch axes acceleration autopilot with appropriate state feedbacks. The plant is a 4th system which makes it hard to arrange how to intervene open loop poles in an artful way. Hence, the dominant poles of the closed loop system are assigned considering the

desired transient response of a similar 2nd order system. The recessive poles are kept at the same location in the s-plane to save the control authority mostly for the dominant pole assignment and roll stabilization.

Transient response characteristics are settled with the following definitions

- **Rise Time:** In this thesis, rise time is defined as time required for the response to rise from 10% to 90%.

$$t_r = \tan^{-1} \left(-\frac{\sqrt{1-\zeta^2}}{\zeta\omega_d} \right) \quad (\text{A.7})$$

where ω_d is defined as $\omega_d = \omega_n \sqrt{1-\zeta^2}$

- **Maximum Percent Overshoot:** The maximum overshoot is the maximum peak value of the response curve measured from the unity.

$$M_p = e^{\frac{-\zeta\pi}{\sqrt{1-\zeta^2}}} \quad (\text{A.8})$$

The desired response is specified as $t_r \leq 0.5s$ and $M_p \leq 7\%$ then, the corresponding ζ and ω_n values are obtained which provides the required performance using equations (3.7) and (3.8). The 2nd order system which is used to locate the dominant poles is formed using (3.9).

$$H(s) = \frac{\omega_n^2}{s^2 \pm 2\zeta\omega_n s + \omega_n^2} \quad (\text{A.9})$$

A sample pole-zero map of the pole assignment with the explained method is shown in Figure A.2-2.

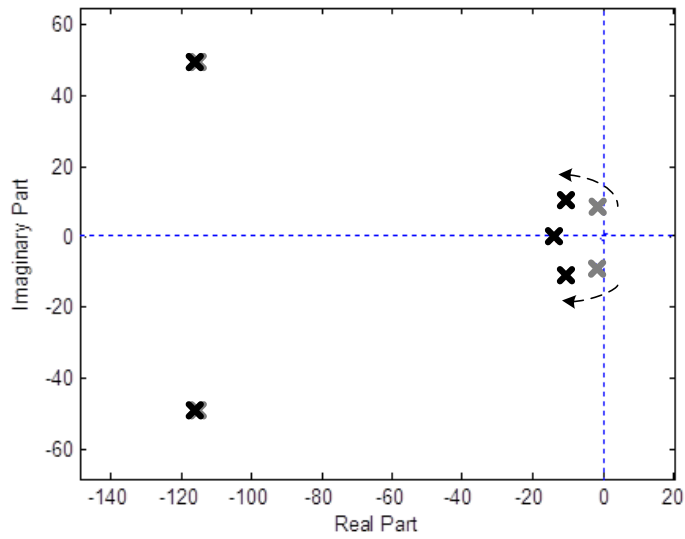


Figure A.2-2 The pole-zero map for acceleration autopilot

In Figure A.2-2, the gray markers represent the open loop poles of the system and the black markers represent the closed-loop system. In the stable part of the s-domain, as the poles are moved away from the imaginary axis, the response become faster; as the poles are moved away from the real axis, oscillations of the response increase as well as the system becomes faster.

As can be seen in the given pole-zero map, the closed-loop poles are placed such that the response become faster with an intended overshoot. The integral controller which is included to eliminate the steady state error implies an additional pole in the closed-loop. This additional pole enhances the degree of freedom of the control and eases to shape the root locus in a desired way.